



HAL
open science

The Interaction of Two Unsteady Point Vortex Sources in a Deformation Field in 2D Incompressible Flows

Armand Vic, Xavier Carton, Jonathan Gula

► **To cite this version:**

Armand Vic, Xavier Carton, Jonathan Gula. The Interaction of Two Unsteady Point Vortex Sources in a Deformation Field in 2D Incompressible Flows. *Regular and Chaotic Dynamics*, 2021, 26, pp.618-646. 10.1134/S1560354721060034 . insu-03683247

HAL Id: insu-03683247

<https://insu.hal.science/insu-03683247>

Submitted on 2 May 2023

HAL is a multi-disciplinary open access archive for the deposit and dissemination of scientific research documents, whether they are published or not. The documents may come from teaching and research institutions in France or abroad, or from public or private research centers.

L'archive ouverte pluridisciplinaire **HAL**, est destinée au dépôt et à la diffusion de documents scientifiques de niveau recherche, publiés ou non, émanant des établissements d'enseignement et de recherche français ou étrangers, des laboratoires publics ou privés.

The Interaction of Two Unsteady Point Vortex Sources in a Deformation Field in 2D Incompressible Flows

Vic Armand¹, Carton Xavier¹, Gula Jonathan^{1,2}

¹ Univ. Brest, CNRS, Ifremer, IRD, Laboratoire d'Océanographie Physique et Spatiale (LOPS), IUEM, 29280, Plouzané, France

² Institut Universitaire de France (IUF), 75005, Paris, France

Email addresses : armand.vic@univ-brest.fr ; xcarton@univ-brest.fr ; jonathan.gula@univ-brest.fr

Abstract :

Taking into account the coupling of the ocean with the atmosphere is essential to properly describe vortex dynamics in the ocean. The forcing of a circular eddy with the relative wind stress curl leads to an Ekman pumping with a nonzero area integral. This in turn creates a source or a sink in the eddy. We revisit the two point vortex-source interaction, now coupled with an unsteady wind, leading to a time-varying circulation and source strength. Firstly, we recover the various fixed points of the two vortex-source system, and we calculate their stability. Then we show the effect of a weak amplitude, subharmonic, or harmonic time variation of the wind, leading to a similar variation of the circulation and the source strength of the vortex sources. We use a multiple time scale expansion of the variables to calculate the long time variation of these vortex trajectories around neutral fixed points. We study the amplitude equation and obtain its solution. We compute numerically the unstable evolution of the vortex sources when the source and circulation have a finite periodic variation. We also assess the influence of this time variation on the dispersion of a passive tracer near these vortex sources.

Keywords : wind oceanic vortex interaction, vortex-source dynamics, system of ODE, equilibrium point and stability, multiple time scale expansion, dispersion of passive tracers

INTRODUCTION

Vortices are essential features in ocean dynamics [1, 2]. They are ubiquitous at least at the ocean surface [3] and they contribute substantially to the meridional heat and momentum transfer. Large oceanic vortices have a moderate Rossby number (the ratio between the Coriolis parameter and the inertial accelerations) and a finite Burger number (which measures the relative influences of global rotation and of fluid stratification). Such vortices have been accurately studied using the quasi-geostrophic (QG) model. In particular, the stability of isolated QG-vortices, and QG-vortex interactions have been investigated, see [4–12]. The simplest vortex interaction occurs between pointwise structures. Point vortex interaction has also been the subject of many studies, investigating in particular the onset of Hamiltonian chaos [13–19]).

Recent studies of oceanic vortices have shown the importance of taking into account the oceanic flow in the atmospheric forcing terms for a proper evaluation of the strength and durability of these vortices [20]. Also, the Gulf Stream latitude of detachment from the coast and its eastward extent, have been proved sensitive to a wind forcing properly taking into account the presence of vortices [21].

In the present study, we explore the consequence of taking into account the relative wind stress on a vortex. We show that a source/sink flow component appears in the vortex flow. We analyse the interaction of two identical point vortex-sources (or vortex-sinks) in an external deformation flow mimicking the influence of neighboring vortices. The motion of point-vortex sources has already

been addressed in previous studies [22, 23]. The first paper lists the integral invariants of the problem and the cases of integrability of the equations. It then describes the motion of two point vortex-sources. The second paper lists the fixed points of two vortex-sources in a deformation flow and briefly addresses the case of a time varying deformation flow.

In section 1, we complement these studies by considering that, due to the interaction of the wind with the vortex-sources, both the source strength and the vortex circulation vary periodically in time. In section 2, we look at the dynamical system and compute the equilibrium points and there stability. In section 3, we follow the method of [14], a multiple time expansion, to obtain an amplitude equation for the slow time variation of the position of each vortex source and we study this amplitude equation with respect to this time variation of the vortex source and circulation. Finally, we model numerically the evolution of the two point vortex-sources and of passive particles moving around them in section 4. Conclusions, perspectives and physical interpretations are finally provided in a last section.

1. MODELLING THE RELATIVE ATMOSPHERIC FORCING OF A VORTEX FLOW

1.1. Basic equations

The linearized momentum equations on the f -plane for an ocean, forced by a wind stress $\vec{\tau}$ are :

$$\begin{cases} \partial_t u - f_0 v = (-1/\rho_0) \partial_x p + (\tau_x/\rho_0) - ku \\ \partial_t v + f_0 u = (-1/\rho_0) \partial_y p + (\tau_y/\rho_0) - kv \end{cases} \quad (1.1)$$

where k is a friction coefficient (a necessary loss of energy of this ocean to balance the momentum input by the wind).

For low frequency, low Rossby number motions, we neglect the relative acceleration and replace the pressure gradient by a geostrophic velocity.

$$\begin{cases} -f_0 v &= -f_0 v_g + (\tau_x/\rho_0) - ku \\ f_0 u &= f_0 u_g + (\tau_y/\rho_0) - kv. \end{cases} \quad (1.2)$$

Using the subscript ‘‘a’’ for the ageostrophic velocity $u_a = u - u_g$, we have

$$\begin{cases} -f_0 v_a + ku &= (\tau_x/\rho_0) \\ f_0 u_a + kv &= (\tau_y/\rho_0). \end{cases} \quad (1.3)$$

Taking the curl of the system (1.3) we obtain

$$f_0 \vec{\nabla} \cdot \vec{u}_a + k \vec{z} \cdot \vec{\nabla} \times \vec{u} = \vec{z} \cdot \vec{\nabla} \times \vec{\tau} / \rho_0. \quad (1.4)$$

Thus we see that the wind stress curl $\vec{\tau}$ can have an influence on both the vorticity $\omega = \nabla \times u$ and the velocity divergence $\nabla \cdot u$ (the source-sink term). In particular, if the wind has a steady or a time-varying component, it will induce steady or time-varying velocity divergence and curl. This source-sink effect is next explained in more details.

1.2. The relative wind stress curl

Recent work [20] has shown that, for the ocean mesoscales, and in particular for the dynamics of oceanic vortices, the wind stress should be computed using the relative velocity of the air to the ocean.

$$\vec{\tau} = \rho_{\text{air}} C_D |\vec{u}_{\text{air}} - \vec{u}_{\text{ocean}}| (\vec{u}_{\text{air}} - \vec{u}_{\text{ocean}}), \quad (1.5)$$

– hereafter referred to as relative wind stress – rather than the total wind velocity

$$\vec{\tau}_a = \rho_{\text{air}} C_D |\vec{u}_{\text{air}}| \vec{u}_{\text{air}} \quad (1.6)$$

(the absolute wind stress). In these expressions, ρ_{air} is the density of the air, C_D is the drag coefficient (about $1.5 \cdot 10^{-3}$ for $|\vec{u}_{\text{air}}| = 15$ m/s), \vec{u}_{air} is the wind velocity, and \vec{u}_{ocean} is the velocity

of the oceanic currents.

In what follows, we estimate the difference induced by taking the relative rather than the absolute wind stress, using a simple configuration :

- a zonal and horizontally sheared wind $\vec{u}_{\text{air}} = (U_0 - qy)\vec{i}$.
- a circular vortex oceanic flow $\vec{u}_{\text{ocean}} = \Upsilon r \vec{e}_\theta$ for $0 < r < R$ (we neglect the vortex deformation due to the wind, in this simple estimate), where \vec{e}_θ is the tangential vector to the circle, R is the vortex radius and Υ (capital upsilon) is the vortex rotation rate.

From there, we can compute the relative wind stress through

$$\vec{u}_{\text{air}} - \vec{u}_{\text{ocean}} = \begin{pmatrix} U_0 - qy + \Upsilon r \sin(\theta) \\ -\Upsilon r \cos(\theta) \end{pmatrix} = U_0 \begin{pmatrix} 1 + \frac{\Upsilon - q}{U_0} y \\ -\frac{\Upsilon}{U_0} x \end{pmatrix}, \quad (1.7)$$

so

$$|\vec{u}_{\text{air}} - \vec{u}_{\text{ocean}}| = U_0 \sqrt{\left(1 + \frac{\Upsilon - q}{U_0} y\right)^2 + \frac{\Upsilon^2}{U_0^2} x^2}. \quad (1.8)$$

We next assume that $qR/U_0 \sim \Upsilon R/U_0 \sim \varepsilon$ (in practice on the order of 10^{-2}). Setting

$$\varepsilon\alpha = \frac{\Upsilon - q}{U_0} y, \quad \varepsilon\gamma = \frac{\Upsilon}{U_0} x, \quad (1.9)$$

we obtain via a Taylor expansion that

$$\vec{\tau} = \tau_0 \begin{pmatrix} 1 + 2\varepsilon\alpha + \varepsilon^2(\alpha^2 + \frac{\gamma^2}{2}) \\ -\varepsilon\gamma - \varepsilon^2\alpha\gamma \end{pmatrix}, \quad (1.10)$$

where $\tau_0 = \rho_{\text{air}} C_D U_0^2$.

The wind stress curl is evaluated at orders 0, ε , ε^2 . The first two orders give

$$\nabla \times \begin{pmatrix} \tau_0 \\ 0 \end{pmatrix} = 0, \quad \nabla \times \begin{pmatrix} 2\varepsilon\alpha \\ -\varepsilon\gamma \end{pmatrix} = -\tau_0 \frac{2q + \Upsilon}{U_0}. \quad (1.11)$$

The effect of the atmosphere-ocean coupling becomes apparent. In the absence of wind shear ($q = 0$), the curl of τ at order ε^1 would be null for an absolute wind stress.

The presence of a wind stress curl leads to an Ekman vertical velocity (Ekman pumping) :

$$w_E = \frac{1}{\rho_o} \nabla \times \frac{\vec{\tau}}{f_0}, \quad (1.12)$$

where ρ_o is the seawater density.

It should be noted that, from this expression, one can compare the effect of the relative wind stress to the effect of the Earth's curvature on the Ekman vertical velocity. The former is

$$w_E(\text{air} - \text{ocean}) = -\frac{\rho_{\text{air}}}{\rho_{\text{ocean}}} C_D U_0 \frac{\Upsilon + 2q}{f_0}, \quad (1.13)$$

while the latter is

$$w_E(\beta) = -\beta \frac{\rho_{\text{air}}}{\rho_{\text{ocean}}} C_D \frac{U_0^2}{f_0^2}. \quad (1.14)$$

Using $\Upsilon \sim q \sim 10^{-5} \text{s}^{-1}$ and $U_0 = 15 \text{ m/s}$, one obtains that the Ekman vertical velocity due to the absolute wind stress is about 30% of the one due to the relative wind stress.

1.3. Ekman pumping and point vortex sources

We next calculate the source/sink magnitude S_0 associated with the Ekman vertical velocity. To compute order of magnitude, we here assume that the source/sink term S_0 and the circulation of the vortex Γ_0 are decorrelated. Assuming that the Ekman pumping is uniform over the vortex area, we can calculate an order of magnitude for $S_0 = S\pi R^2 w_E$.

We can also compare the radial velocity thus created $v_R = S_0/(2\pi RH)$ to the vortex velocity $v_\theta = \Upsilon R$. With $R = 15$ km, the radial velocity is on the order of $2.25 \cdot 10^{-3}$ m/s while the azimuthal velocity is $v_\theta = 0.15$ m/s. The source/sink magnitude S_0 is therefore about 1.5% that of the circulation Γ_0 .

Note that such vortices are not identical to vortices in a stratified ocean with free density interfaces. Such vortices, in a steady circular configuration, would have no vertical velocity.

We hereafter assume that the vortex-sources are point vortex-sources. This is a strong assumption which would, in practice, suppress the effect of the wind stress curl. In fact this point-vortex assumption means that we only study the vortex motion and not its deformation.

2. INTERACTION OF TWO POINT VORTEX SOURCES

The study of this interaction proceeds in two steps. Firstly, we consider a steady wind and so constant circulation Γ_0 and source/sink magnitude S_0 . Secondly, we consider a time oscillating circulation $\Gamma(t)$ and we address the vortex motion via a multiple time scale method.

2.1. Equations of motion

We consider two similar vortex-sources in the plane (see Fig. 1) on which an external deformation flow acts. This external flow mimicks the effect of surrounding vortices or currents. This problem is analytically tractable in particular if we assume central symmetry. Using this symmetry, we derive the equations for only one of the two vortex-sources. Vortex-source 1 has polar coordinates (r, θ) and by symmetry, the second vortex-source has $(r, \theta + \pi)$.

Vortex-source 1 is submitted to the influence of :

- vortex-source 2 :

$$\begin{cases} \dot{r} = \frac{S_0}{2\pi(2r)} \\ r\dot{\theta} = \frac{\Gamma_0}{2\pi(2r)} \end{cases} \quad (2.1)$$

- the external deformation flow composed of a global rotation and a strain :

$$\begin{cases} \dot{r} = rA \cos(2\theta) \\ r\dot{\theta} = r\Omega - rA \sin(2\theta) \end{cases} \quad (2.2)$$

The vortex-source motion is therefore governed by :

$$\begin{cases} \dot{r} = \frac{S_0}{4\pi r} + rA \cos(2\theta) \\ \dot{\theta} = \frac{\Gamma_0}{4\pi r^2} + \Omega - A \sin(2\theta) \end{cases} \quad (2.3)$$

All the physical parameters $(S_0, \Gamma_0, \Omega, A)$ are assumed non zero.

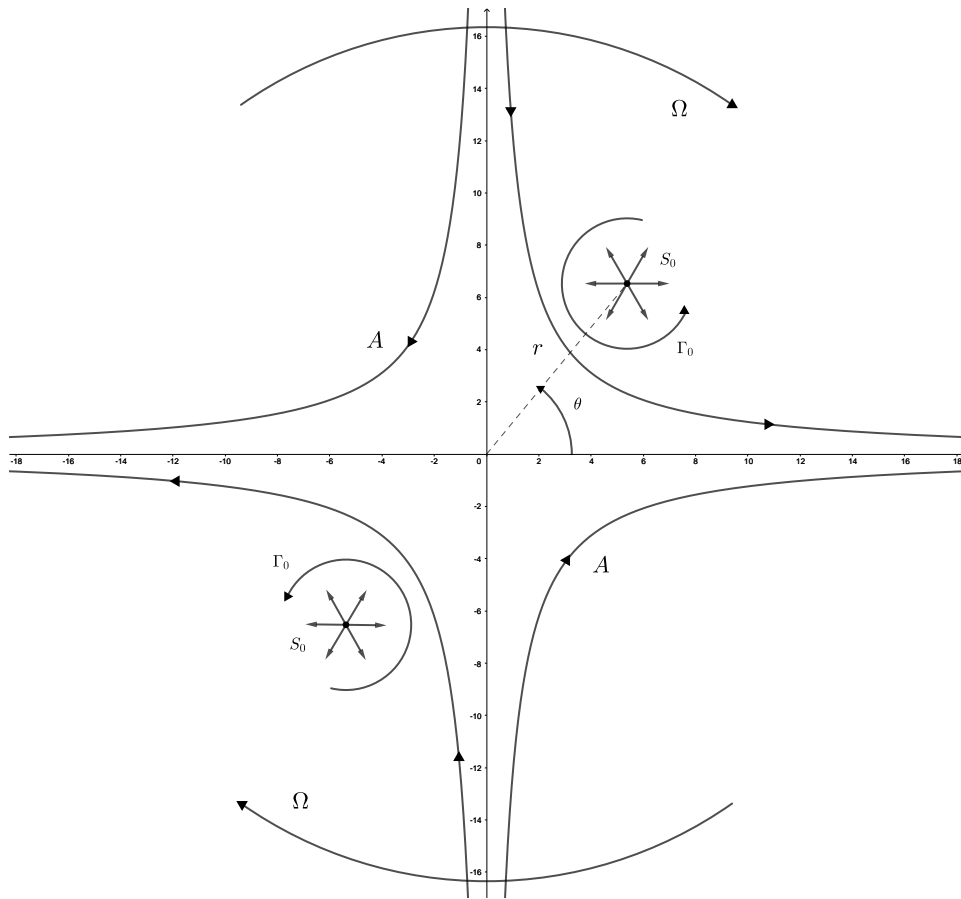


Fig. 1. The two similar point vortex-sources in a deformation flow.

2.2. Equilibrium points and stability

2.2.1. Preliminaries

The equilibrium points $(r_0, \theta_0) \in \mathbf{R}_+^* \times [-\frac{\pi}{4}, \frac{3\pi}{4}[$ satisfy :

$$\begin{cases} \frac{S_0}{4\pi r_0} + r_0 A \cos(2\theta_0) = 0 \\ \frac{\Gamma_0}{4\pi r_0^2} + \Omega - A \sin(2\theta_0) = 0 \end{cases} \quad (2.4)$$

Let (r_0, θ_0) be an equilibrium. To determine its stability, we calculate the Jacobian matrix $D_{(r_0, \theta_0)} \mathbf{u}$ from the velocity field :

$$\mathbf{u}(r, \theta) = \begin{pmatrix} \frac{S_0}{4\pi r} + r A \cos(2\theta) \\ \frac{\Gamma_0}{4\pi r^2} + \Omega - A \sin(2\theta) \end{pmatrix}, \quad (2.5)$$

$$D_{(r_0, \theta_0)} \mathbf{u} = \begin{pmatrix} -\frac{S_0}{2\pi r_0^2} & -\frac{\Gamma_0}{2\pi r_0} - 2r_0 \Omega \\ \frac{-\Gamma_0}{2\pi r_0^3} & \frac{S_0}{2\pi r_0^2} \end{pmatrix}. \quad (2.6)$$

Its characteristic polynomial is

$$\chi(X) = X^2 - \frac{S_0^2 + \Gamma_0^2 + 4\pi r_0^2 \Gamma_0 \Omega}{4\pi^2 r_0^4}. \quad (2.7)$$

Depending on the sign of

$$\Delta_0 = S_0^2 + \Gamma_0^2 + 4\pi r_0^2 \Gamma_0 \Omega, \quad (2.8)$$

we have a neutral (or center) equilibrium point (if $\Delta_0 < 0$) or a saddle equilibrium point if $\Delta_0 > 0$.

Since saddle points are unstable, and since we wish to describe the long term evolution of the weakly perturbed vortex-source system (see the following section), we only consider neutral equilibria. A necessary condition for the existence of a center then appears :

$$\Gamma_0 \Omega < 0. \quad (2.9)$$

(if $\Gamma_0 \Omega > 0$, the vortices diverge to infinity along the x or y axis). Hereafter, we assume that this condition is satisfied (unless otherwise stated).

Remark 1. Considering the oceanic case, where $S_0 \ll \Gamma_0$, the condition on Δ_0 for the existence of a center, becomes approximately $\Gamma_0^2 + 4\pi r_0^2 \Gamma_0 \Omega < 0$.

2.2.2. Existence of an neutral equilibrium point

Firstly, we calculate the position of the equilibria from the system (2.4) :

$$\begin{cases} r_0^2 A \cos(2\theta_0) = -\frac{S_0}{4\pi} \\ r_0^2 A \sin(2\theta_0) = \frac{\Gamma_0}{4\pi} + r_0^2 \Omega \end{cases} \quad (2.10)$$

implicates $\tan(2\theta_0) = -\frac{\Gamma_0 + 4\pi r_0^2 \Omega}{S_0}$. Because the function $]-\frac{\pi}{2}, \frac{\pi}{2}[\rightarrow \mathbf{R}, x \mapsto \tan(2x)$ is not injective, we cannot decide analytically (through this research of necessary conditions method) if we have

$$\theta_0 = -\frac{1}{2} \arctan \left[\frac{\Gamma_0 + 4\pi r_0^2 \Omega}{S_0} \right], \quad (2.11)$$

or

$$\theta_0 = -\frac{1}{2} \arctan \left[\frac{\Gamma_0 + 4\pi r_0^2 \Omega}{S_0} \right] + \frac{\pi}{2}. \quad (2.12)$$

But this is not a numerical difficulty since the equilibrium points are clear in a streamfunction plot.

Squaring and summing the two equations in (2.10) gives a biquadratic equation in r_0

$$r_0^4 (\Omega^2 - A^2) + \frac{\Gamma_0 \Omega}{2\pi} r_0^2 + \frac{S_0^2 + \Gamma_0^2}{16\pi^2} = 0. \quad (2.13)$$

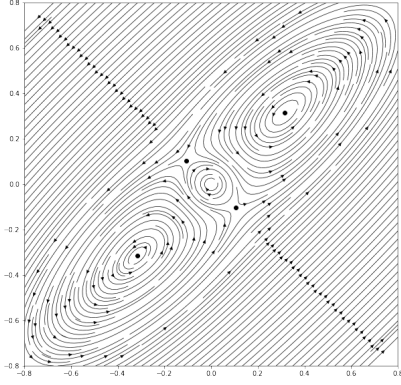
From this equation, several equilibria can be found (they are detailed in Appendix A). The only equilibrium point which is a center is determined by :

$$r_0 = \sqrt{\frac{-\Gamma_0 \Omega + \sqrt{\Delta'}}{4\pi (\Omega^2 - A^2)}} \quad \text{and} \quad \theta_0 = \frac{1}{2} \arctan \left[\frac{\Gamma_0 A^2 - \Omega \sqrt{\Delta'}}{S_0 (\Omega^2 - A^2)} \right] \left(+\frac{\pi}{2} \right), \quad (2.14)$$

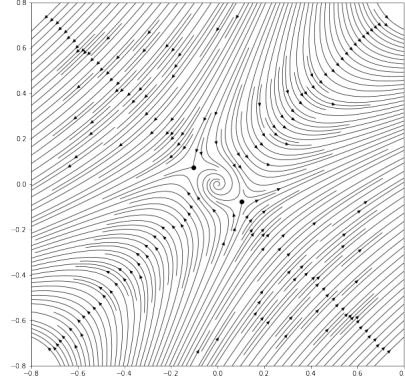
where $\Delta' = A^2 (S_0^2 + \Gamma_0^2) - S_0^2 \Omega^2 = S_0^2 (A^2 - \Omega^2) + A^2 \Gamma_0^2$ and where the additional $+\frac{\pi}{2}$ depends on the sign of S_0 . This is valid under the conditions

$$A^2 < \Omega^2 < A^2 \left(1 + \frac{\Gamma_0^2}{S_0^2} \right) \quad \text{and} \quad \Gamma_0 \Omega < 0. \quad (2.15)$$

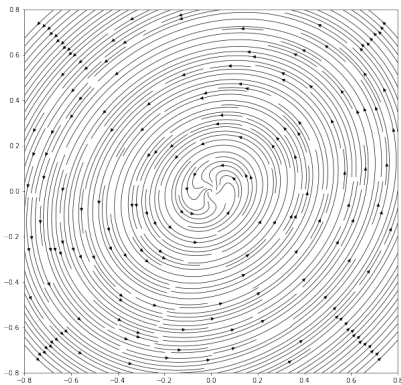
Remark 2. These conditions do not depend on the sign of S_0 . This will allow us to choose S_0 as a source or a sink with the same intensity.



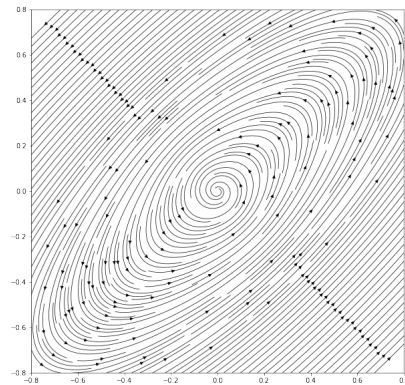
$$\Gamma_0 = -0.5, S_0 = 0.01, \Omega = 1, A = 0.8$$



$$\Gamma_0 = -0.5, S_0 = -0.1, \Omega = 1, A = 1.5$$



$$\Gamma_0 = -0.5, S_0 = -0.3, \Omega = 8.5, A = 1.5$$



$$\Gamma_0 = 0.5, S_0 = -0.3, \Omega = 8.5, A = 1.5$$

Fig. 2. Vortex-source trajectories for different sets of physical parameter values. Neutral equilibrium points (centers) appear only in the configuration where the conditions (2.15) are fulfilled (see upper left panel). The upper right panel shows a case with a strong strain field; the lower two cases have fast global rotation with either like-signed or opposite-signed circulation and source intensity.

The various equilibria and their nature depending on the four physical parameters are shown in Fig. 2. This figure shows the presence of an attractive or of a repulsive center at the origin of the plane when the source flow is strong (this equilibrium will not be considered further because it corresponds to the final position of the two vortex-sources after a merging event). Two saddle points exist when the source flow is weak and when the strain flow is strong. Finally, two centers appear for weak external flow and weak source intensity, and when conditions (2.15) are satisfied.

Remark 3. With $\Gamma_0 < 0, S_0 < 0, \Omega > A > 0$, the oceanographic limit $|S_0| \ll |\Gamma_0|$ leads to the following approximation for the center position: $\theta_0 \approx \pi/4, r_0 \approx \sqrt{-\Gamma_0/[4\pi(\Omega - A)]}$. Note that though S_0 is not infinitesimal in Fig. 2, the orientation of the centers correspond to this solution in the upper left case.

3. VORTEX MOTION WITH UNSTEADY CIRCULATION AND SOURCE-SINK MAGNITUDE

This section is devoted to the motion of a source-sink pair with a periodic circulation and source magnitude, due to the effect of an equally periodic wind stress. This wind stress is assumed to have a dominant steady component and a weak periodic component. In this section, we first address the

case of a sub-harmonic time variation of Γ and of S with respect to the period of rotation of a vortex-source around the neutral equilibrium point.

3.1. Weakly nonlinear evolution of the vortex pair displaced from a center with a sub-harmonic variation of circulation and source

We consider a center point defined by Eq. (2.14) that we slightly perturb from its equilibrium position. Computed from Eq. (2.7), the natural pulsation of the motion around this center is

$$\omega_0 = \frac{\sqrt{-[S_0^2 + \Gamma_0^2 + 4\pi r_0^2 \Gamma_0 \Omega]}}{2\pi r_0^2}. \quad (3.1)$$

3.1.1. Multiple time scale development

In this subsection, we assume that the wind stress leads to a sub-harmonic variation of system (2.3) with circulation and source-sink magnitude :

$$\begin{cases} \Gamma(t) = \Gamma_0 (1 + \varepsilon^2 \delta \cos(2\omega_0 t)) \\ S(t) = S_0 (1 + \varepsilon^2 \delta \cos(2\omega_0 t)) \end{cases} \quad (3.2)$$

The algebra for this sub-harmonic case is detailed here and in Appendix B. To simplify notations, we introduce the constants

$$\begin{cases} a = \frac{S_0}{2\pi r_0^2} = -2A \cos(2\theta_0) \\ b = 2 \left(\Omega + \frac{\Gamma_0}{4\pi r_0^2} \right) = 2A \sin(2\theta_0) \\ c = \frac{\Gamma_0}{2\pi r_0^2} \end{cases} \quad (3.3)$$

such that $a^2 + bc = -\omega_0^2$.

Remark 4. For an oceanic point vortex-source, $|S_0| \sim 1.5\%|\Gamma_0|$ so $a \ll b$ and $a \ll c$. Although this is not done here, we could use this to make approximations in the following computations. In the Appendix B, we can see that the quotient rates a/b and a/c appear frequently.

The equation of motion is expanded at higher order in ε than in the previous section. Close to (r_0, θ_0) , we expand in ε the time $t = t_0 + \varepsilon t_1 + \varepsilon^2 t_2 + \varepsilon^3 t_3$ and the dynamical variables :

$$\begin{cases} r = r_0 + \varepsilon r_1 + \varepsilon^2 r_2 + \varepsilon^3 r_3 \\ \theta = \theta_0 + \varepsilon \theta_1 + \varepsilon^2 \theta_2 + \varepsilon^3 \theta_3 \end{cases} \quad (3.4)$$

Once substituted in the equation of motion (2.3) we obtain :

- Equations for r :

$$\begin{aligned} \partial_t r &= \varepsilon (\partial_{t_0} r_1) + \varepsilon^2 (\partial_{t_0} r_2 + \partial_{t_1} r_1) + \varepsilon^3 (\partial_{t_0} r_3 + \partial_{t_1} r_2 + \partial_{t_2} r_1) \\ &= \underbrace{\frac{S_0}{4\pi r_0}}_{=0} + Ar_0 \cos(2\theta_0) + \varepsilon [-ar_1 - b(r_0\theta_1)] \end{aligned} \quad (3.5)$$

$$+ \varepsilon^2 \left[-ar_2 - b(r_0\theta_2) + \frac{a\delta r_0}{2} \cos(2\omega_0 t_0) + \frac{a}{2r_0} r_1^2 + \frac{a}{r_0} (r_0\theta_1)^2 - \frac{b}{r_0} r_1 (r_0\theta_1) \right] \quad (3.6)$$

$$\begin{aligned}
& + \varepsilon^3 \left[-ar_3 - b(r_0\theta_3) + \frac{a}{r_0}r_1r_2 - \frac{ar_1^3}{2r_0^2} - \frac{a\delta}{2}r_1 \cos(2\omega_0t_0) - a\delta r_0\omega_0t_1 \sin(2\omega_0t_0) \right. \\
& \left. - \frac{b}{r_0}(r_2(r_0\theta_1) + r_1(r_0\theta_2)) + \frac{a}{r_0^2}r_1(r_0\theta_1)^2 + \frac{2a}{r_0}(r_0\theta_1)(r_0\theta_2) + \frac{2b}{3r_0^2}(r_0\theta_1)^3 \right]
\end{aligned} \tag{3.7}$$

- Equations for θ :

$$\begin{aligned}
\partial_t(r_0\theta) &= \varepsilon [\partial_{t_0}(r_0\theta_1)] + \varepsilon^2 [\partial_{t_0}(r_0\theta_2) + \partial_{t_1}(r_0\theta_1)] \\
&= \underbrace{\frac{\Gamma_0}{4\pi r_0} + r_0\Omega - Ar_0 \sin(2\theta_0)}_{=0} + \varepsilon [-cr_1 + a(r_0\theta_1)]
\end{aligned} \tag{3.8}$$

$$+ \varepsilon^2 \left[-cr_2 + a(r_0\theta_2) + \frac{c\delta r_0}{2} \cos(2\omega_0t_0) + \frac{3c}{2r_0}r_1^2 + \frac{b}{r_0}(r_0\theta_1)^2 \right] \tag{3.9}$$

$$\begin{aligned}
& + \varepsilon^3 \left[-cr_3 + a(r_0\theta_3) - c\delta r_1 \cos(2\omega_0t_0) + \frac{3c}{r_0}r_1r_2 + \frac{2b}{r_0}(r_0\theta_1)(r_0\theta_2) \right. \\
& \left. - \frac{2c}{r_0^2}r_1^3 - \frac{2a}{3r_0^2}(r_0\theta_1)^3 - c\delta r_0\omega_0t_1 \sin(2\omega_0t_0) \right]
\end{aligned} \tag{3.10}$$

By gathering terms at each order we obtain :

At order ε^1 As expected, we recover from Eqs. (3.5) and (3.8) the unforced harmonic oscillator (the forcing appears only at order ε^2).

$$\begin{cases} \partial_{t_0}r_1 = -ar_1 - b(r_0\theta_1) \\ \partial_{t_0}(r_0\theta_1) = -cr_1 + a(r_0\theta_1) \end{cases} \tag{3.11}$$

with solution

$$r_1 = C_{1,1}(t_2, t_3) e^{i\omega_0t_0} + \overline{C_{1,1}}(t_2, t_3) e^{-i\omega_0t_0}. \tag{3.12}$$

Hereafter, the second term is denoted c. c for “complex conjugate”.

$$r_0\theta_1 = D_{1,1}(t_2, t_3) e^{i\omega_0t_0} + \text{c. c.} \tag{3.13}$$

with

$$D_{1,1}(t_2, t_3) = \mu_1 C_{1,1}(t_2, t_3), \tag{3.14}$$

where $\mu_1 = -\frac{a+i\omega_0}{b}$.

At order ε^2 Equations (3.6) and (3.9) contain nonlinear terms. The absence of linear growth of the solution leads to $\partial_{t_1}C_{1,1} = \partial_{t_1}r_1 = 0$:

$$\begin{cases} \partial_{t_0}r_2 = -ar_2 - b(r_0\theta_2) + f_2(t_0, t_1, t_2, t_3) \\ \partial_{t_0}(r_0\theta_2) = -cr_2 + a(r_0\theta_2) + g_2(t_0, t_1, t_2, t_3) \end{cases} \tag{3.15}$$

with f_2 and g_2 are two functions defined by :

$$\begin{cases} f_2(t_0, t_1, t_2, t_3) = \frac{a\delta r_0}{2} \cos(2\omega_0t_0) + \frac{a}{2r_0}r_1^2 + \frac{a}{r_0}(r_0\theta_1)^2 - \frac{b}{r_0}r_1(r_0\theta_1) \\ g_2(t_0, t_1, t_2, t_3) = \frac{c\delta r_0}{2} \cos(2\omega_0t_0) + \frac{3c}{2r_0}r_1^2 + \frac{b}{r_0}(r_0\theta_1)^2 \end{cases} \tag{3.16}$$

This leads to the solution :

$$\begin{cases} r_2 &= C_{2,0}|C_{1,1}|^2 + C_{2,1} e^{i\omega_0t_0} + \text{c. c.} + (C_{2,2,1} + C_{2,2,2}C_{1,1}^2) e^{2i\omega_0t_0} + \text{c. c.} \\ (r_0\theta_2) &= D_{2,0}|C_{1,1}|^2 + D_{2,1} e^{i\omega_0t_0} + \text{c. c.} + (D_{2,2,1} + D_{2,2,2}C_{1,1}^2) e^{2i\omega_0t_0} + \text{c. c.} \end{cases} \tag{3.17}$$

where $C_{2,0}$, $C_{2,2,1}$, $C_{2,2,2}$, $D_{2,0}$, $D_{2,2,1}$, $D_{2,2,2}$ are complex constants. Their values are computed and details are given in Appendix B.

At order ε^3 Equations (3.7) and (3.10) lead to the following system of equations :

$$\begin{cases} \partial_{t_0} r_3 = -ar_3 - b(r_0\theta_3) + f_3(t_0, t_1, t_2, t_3) \\ \partial_{t_0} (r_0\theta_3) = -cr_3 + a(r_0\theta_3) + g_3(t_0, t_1, t_2, t_3) \end{cases} \quad (3.18)$$

where f_3 and g_3 are the functions :

$$\begin{cases} f_3 = -\partial_{t_2} r_1 + \frac{ar_1 r_2}{r_0} - \frac{ar_1^3}{2r_0^2} - \frac{a\delta r_1 \cos(2\omega_0 t_0)}{2} - \frac{b(r_2(r_0\theta_1) + r_1(r_0\theta_2))}{r_0} + \frac{ar_1(r_0\theta_1)^2}{r_0^2} \\ \quad + \frac{2a(r_0\theta_1)(r_0\theta_2)}{r_0} + \frac{2b(r_0\theta_1)^3}{3r_0^2} - a\delta r_0\omega_0 t_1 \sin(2\omega_0 t_0) \\ g_3 = -\partial_{t_2} (r_0\theta_1) + \frac{3cr_1 r_2}{r_0} - \frac{2cr_1^3}{r_0^2} - c\delta r_1 \cos(2\omega_0 t_0) - \frac{2a(r_0\theta_1)^3}{3r_0^2} + \frac{2b(r_0\theta_1)(r_0\theta_2)}{r_0} \\ \quad - c\delta\omega_0 t_1 \sin(2\omega_0 t_0) \end{cases} \quad (3.19)$$

This yields (see Appendix B) a differential equation on $C_{1,1}(t_2)$, called the amplitude equation. This equation governs the evolution of the amplitude of a perturbation from the vortex-source around the neutral equilibrium point :

$$\partial_{t_2} C_{1,1} = (\underline{\mathbf{V}} + i\underline{\mathbf{VI}}) \delta \overline{C_{1,1}} + (\underline{\mathbf{VII}} + i\underline{\mathbf{VIII}}) |C_{1,1}|^2 C_{1,1}, \quad (3.20)$$

where $\underline{\mathbf{V}}$, $\underline{\mathbf{VI}}$, $\underline{\mathbf{VII}}$, $\underline{\mathbf{VIII}}$ are real constants computed in Appendix B. For $\Gamma_0 = -0.5$, $S_0 = \pm 0.01$, $\Omega = 1$ and $A = 0.8$ (two sets of parameters respecting conditions (2.15), corresponding to the upper left case of Fig. 2, that we generically use in further numerical applications) we have $\underline{\mathbf{V}} \simeq \mp 3.00 \cdot 10^{-3}$, $\underline{\mathbf{VI}} \simeq 1.33 \cdot 10^{-1}$, $\underline{\mathbf{VII}} \simeq \pm 3.77 \cdot 10^{-2}$ and $\underline{\mathbf{VIII}} \simeq 3.35 \cdot 10^{-1}$.

3.1.2. Study of the amplitude equation

To study the slow-time variation of $C_{1,1}$, we set $C_{1,1} = u e^{i\beta}$ or $C_{1,1} = X + iY$ such that $\partial_{t_2} C_{1,1} = (\partial_{t_2} u + iu\partial_{t_2}\beta) e^{i\beta} = \partial_{t_2} X + i\partial_{t_2} Y$ (the polar form is of interest for determine the equilibria; the Cartesian form is simpler to analyse the stability of these equilibria). Using the polar form and separating the real and imaginary parts yields

$$\begin{cases} \partial_{t_2} u \cos \beta - u\partial_{t_2}\beta \sin \beta = u [(\delta \underline{\mathbf{V}} + u^2 \underline{\mathbf{VII}}) \cos \beta + (\delta \underline{\mathbf{VI}} + u^2 \underline{\mathbf{VIII}}) \sin \beta] \\ \partial_{t_2} u \sin \beta + u\partial_{t_2}\beta \cos \beta = u [(\delta \underline{\mathbf{VI}} + u^2 \underline{\mathbf{VIII}}) \cos \beta + (-\delta \underline{\mathbf{V}} + u^2 \underline{\mathbf{VII}}) \sin \beta] \end{cases} \quad (3.21)$$

equivalent to :

$$\begin{pmatrix} \partial_{t_2} u \\ u\partial_{t_2}\beta \end{pmatrix} = u \delta \begin{pmatrix} \cos(2\beta) & \sin(2\beta) \\ -\sin(2\beta) & \cos(2\beta) \end{pmatrix} \begin{pmatrix} \underline{\mathbf{V}} \\ \underline{\mathbf{VI}} \end{pmatrix} + u^3 \begin{pmatrix} \underline{\mathbf{VII}} \\ \underline{\mathbf{VIII}} \end{pmatrix}. \quad (3.22)$$

The equilibria $u_0 e^{i\beta_0}$ of this amplitude equation (see Fig. 3) are, from Eq. (3.22) either $u_0 = 0$ or they are given by

$$\delta \begin{pmatrix} \cos(2\beta_0) & \sin(2\beta_0) \\ -\sin(2\beta_0) & \cos(2\beta_0) \end{pmatrix} \begin{pmatrix} \underline{\mathbf{V}} \\ \underline{\mathbf{VI}} \end{pmatrix} + u_0^2 \begin{pmatrix} \underline{\mathbf{VII}} \\ \underline{\mathbf{VIII}} \end{pmatrix} = 0, \quad (3.23)$$

leading to

$$\beta_0 = \frac{1}{2} \arctan \left[\frac{\underline{\mathbf{VII}} \underline{\mathbf{VI}} - \underline{\mathbf{V}} \underline{\mathbf{VIII}}}{\underline{\mathbf{VIII}} \underline{\mathbf{VI}} + \underline{\mathbf{V}} \underline{\mathbf{VII}}} \right] \pm \frac{\pi}{2} \simeq 3.86^\circ \pm 90^\circ, \quad (3.24)$$

$$u_0 = \sqrt{\delta} \left(\frac{\mathbb{V}^2 + \mathbb{VI}^2}{\mathbb{VII}^2 + \mathbb{VIII}^2} \right)^{\frac{1}{4}} \simeq 0.6293\sqrt{\delta}. \quad (3.25)$$

(where the numerical applications are done for our choice of physical parameters $\Gamma_0 = -0.5$, $S_0 = \pm 0.01$, $\Omega = 1$ and $A = 0.8$).

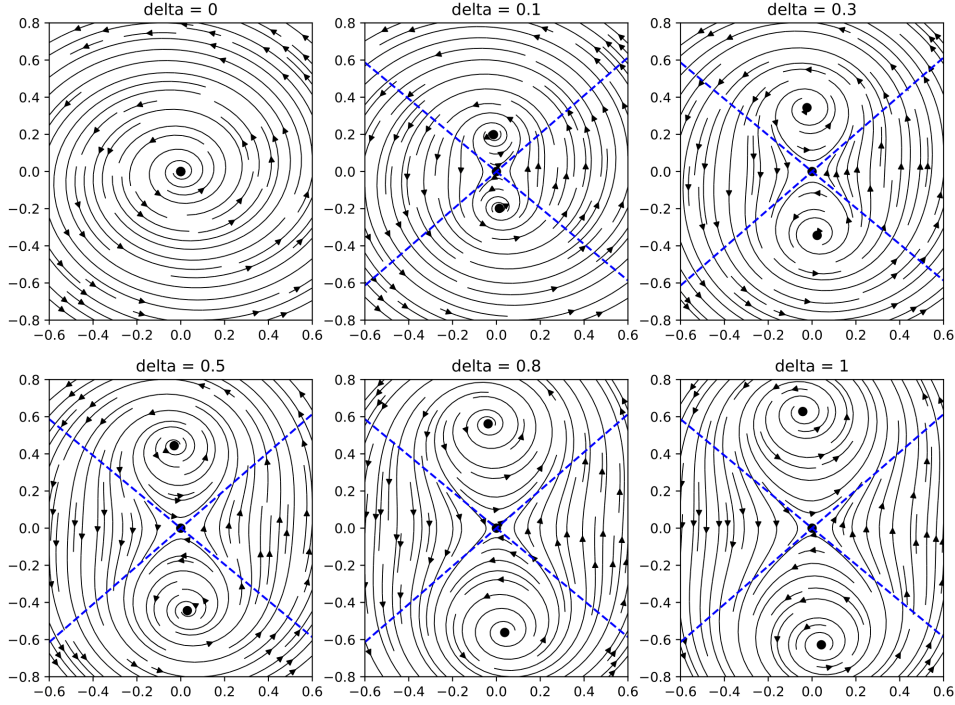


Fig. 3. Slow time evolution of $C_{1,1}(t_2) = X(t_2) + iY(t_2)$ for different values of δ . The blue dashed lines indicate the eigen-directions of stability of the saddle equilibrium point $(0, 0)$. Here $S_0 = +0.01$, the other equilibrium points are repulsive.

The stability analysis of these equilibria is easier calculated in cartesian coordinates :

$$\begin{cases} \partial_{t_2} X = (\mathbb{V}\delta + \mathbb{VII}(X^2 + Y^2)) X + (\mathbb{VI}\delta - \mathbb{VIII}(X^2 + Y^2)) Y \\ \partial_{t_2} Y = (\mathbb{VI}\delta + \mathbb{VIII}(X^2 + Y^2)) X + (-\mathbb{V}\delta + \mathbb{VII}(X^2 + Y^2)) Y \end{cases} \quad (3.26)$$

The Jacobian matrix of this system at the equilibrium point $(X_0, Y_0) = (u_0 \cos(\beta_0), u_0 \sin(\beta_0))$ is

$$M = \begin{pmatrix} \delta\mathbb{V} + \mathbb{VII}(3X_0^2 + Y_0^2) - 2X_0Y_0\mathbb{VIII} & \delta\mathbb{VI} - \mathbb{VIII}(X_0^2 + 3Y_0^2) + 2X_0Y_0\mathbb{VII} \\ \delta\mathbb{VI} + \mathbb{VIII}(3X_0^2 + Y_0^2) + 2X_0Y_0\mathbb{VII} & -\delta\mathbb{V} + \mathbb{VII}(X_0^2 + 3Y_0^2) + 2X_0Y_0\mathbb{VIII} \end{pmatrix}. \quad (3.27)$$

For the equilibrium point $(0, 0)$, the computation of the eigenvalues is straightforward : $\pm \delta \sqrt{\mathbb{V}^2 + \mathbb{VI}^2}$ and the eigen-directions of this saddle point are represented in Fig. 3. As δ grows, two attractive or repulsive points appear and separate from each other in the plane. The nature of the centers depends of the sign of S_0 . For this equilibrium, the numerical study of the real parts of the eigenvalues of the

matrix M gives a linear and positive (resp. negative) value when $S_0 = +0.01$ (resp. $S_0 = -0.01$) with 0.02987 (resp. -0.02987) slope with respect to δ . This corresponds to the repulsive (resp. attractive) nature of the two equilibria.

3.2. Harmonic forcing

In this subsection, the time variation of the circulation and source-sink magnitude is

$$\begin{cases} \Gamma(t_0, t_2) = \Gamma_0 (1 + \delta \varepsilon^3 \cos(\omega_0 t_0 + \omega_2 t_2)) \\ S(t_0, t_2) = S_0 (1 + \delta \varepsilon^3 \cos(\omega_0 t_0 + \omega_2 t_2)) \end{cases} \quad (3.28)$$

The multiple time scale expansion leads to the amplitude equation :

$$\partial_{t_2} C_{1,1} = (\text{VII} + i\text{VIII}) |C_{1,1}|^2 C_{1,1} + \frac{(a - i\omega_0) r_0 \delta}{8} e^{i\omega_2 t_2}, \quad (3.29)$$

which is equivalent in polar coordinates ($C_{1,1} = u e^{i\beta}$) to :

$$\begin{pmatrix} \partial_{t_2} u \\ u \partial_{t_2} \beta \end{pmatrix} = u^3 \begin{pmatrix} \text{VII} \\ \text{VIII} \end{pmatrix} - \frac{r_0 \delta}{8} \begin{pmatrix} -\cos(\beta - \omega_2 t_2) & \sin(\beta - \omega_2 t_2) \\ -\sin(\beta - \omega_2 t_2) & \cos(\beta - \omega_2 t_2) \end{pmatrix} \begin{pmatrix} a \\ \omega_0 \end{pmatrix}, \quad (3.30)$$

or in Cartesian coordinates ($C_{1,1} = X + iY$) to

$$\begin{pmatrix} \partial_{t_2} X \\ \partial_{t_2} Y \end{pmatrix} = (X^2 + Y^2) \begin{pmatrix} \text{VII} & -\text{VIII} \\ \text{VIII} & \text{VII} \end{pmatrix} \begin{pmatrix} X \\ Y \end{pmatrix} + \frac{r_0 \delta}{8} \begin{pmatrix} \cos(\omega_2 t_2) & \sin(\omega_2 t_2) \\ \sin(\omega_2 t_2) & -\cos(\omega_2 t_2) \end{pmatrix} \begin{pmatrix} a \\ \omega_0 \end{pmatrix}. \quad (3.31)$$

For $\omega_2 = 0$, finding the equilibrium point $(X_0, Y_0) = (u_0 \cos(\beta_0), u_0 \sin(\beta_0))$ is straightforward (see Figs. 4 and 5) and we have

$$X_0 = \frac{r_0 \delta (-a\text{VII} + \omega_0\text{VIII})}{8u_0^2 (\text{VII}^2 + \text{VIII}^2)}, \quad Y_0 = \frac{r_0 \delta (a\text{VIII} + \omega_0\text{VII})}{8u_0^2 (\text{VII}^2 + \text{VIII}^2)}, \quad (3.32)$$

where

$$u_0^3 = \frac{r_0 \delta}{8} \sqrt{\frac{a^2 + \omega_0^2}{\text{VII}^2 + \text{VIII}^2}}. \quad (3.33)$$

Numerical evaluation gives

$$u_0 \simeq 0.510 \delta^{\frac{1}{3}}, \quad X_0 \simeq 0.506 \delta^{\frac{1}{3}}, \quad Y_0 \simeq \pm 0.062 \delta^{\frac{1}{3}}, \quad (3.34)$$

for $\Gamma_0 = -0.5$, $S_0 = \pm 0.01$, $\Omega = 1$ and $A = 0.8$.

Analysing the stability of this equilibrium point, we find two complex conjugate eigenvalues of the following matrix

$$M = \begin{pmatrix} \text{VII}(3X_0^2 + Y_0^2) - 2\text{VIII}X_0Y_0 & -\text{VIII}(X_0^2 + 3Y_0^2) + 2\text{VII}X_0Y_0 \\ \text{VIII}(3X_0^2 + Y_0^2) + 2\text{VII}X_0Y_0 & \text{VII}(X_0^2 + 3Y_0^2) + 2\text{VIII}X_0Y_0 \end{pmatrix}, \quad (3.35)$$

which are $(X_0^2 + Y_0^2) (2\text{VII} \pm i\sqrt{3\text{VIII}^2 - \text{VII}^2})$. Again, the real parts are positive or negative depending on the sign of S_0 . For the set of parameters we have chosen, it is a repulsive equilibrium point if $S_0 = +0.01$, and it is an attractive equilibrium point if $S_0 = -0.01$, as we can see on Figs. 4 and 5. Around those points, the oscillation pulsation is

$$\tilde{\omega}_2 = (X_0^2 + Y_0^2) \sqrt{3\text{VIII}^2 - \text{VII}^2} = (r_0 \delta)^{\frac{2}{3}} \left(\frac{a^2 + \omega_0^2}{\text{VII}^2 + \text{VIII}^2} \right)^{\frac{1}{3}} \frac{\sqrt{3\text{VIII}^2 - \text{VII}^2}}{4} \simeq 0.150 \delta^{\frac{2}{3}} \quad (3.36)$$

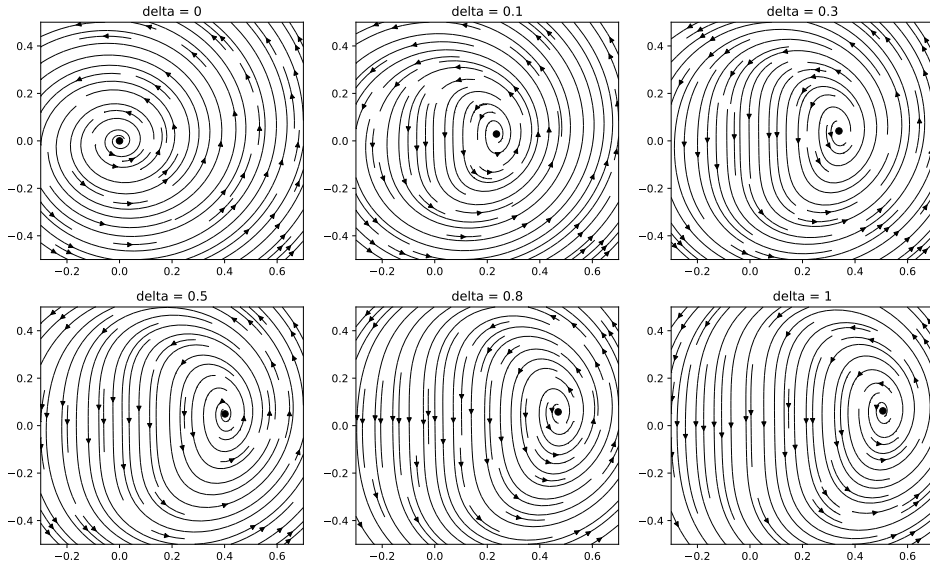


Fig. 4. Slow time evolution of $C_{1,1}(t_2) = X(t_2) + iY(t_2)$ for the harmonic forcing in the case $\omega_2 = 0$ and for $S_0 = +0.01$.

for the set of parameters we chose, independently of the sign of S_0 .

When $\omega_2 \neq 0$, the behaviour of the system changes radically if we are in a source system ($S_0 > 0$) or a sink system ($S_0 < 0$), as we can see on the following figures Figs. 6 and 7 :

4. IMPACT OF THE SOURCE/CIRCULATION VARIABILITY ON THE TRAJECTORIES OF THE VORTEX-SOURCES AND OF PASSIVE TRACERS

In this section, we compute numerically the evolution of the point vortex-sources (or vortex-sinks) and of passive tracers, advected by the total velocity field, when we vary ε . The results are quite similar for the subharmonic or the harmonic case so we will only present the results for the subharmonic variability.

4.1. Point vortex trajectories

Firstly we study the trajectory of the point vortex-sources before considering the evolution of the passive tracers. Figures 8 and 9 are built using a 4th order Runge-Kutta scheme and show the evolution of one of the two point vortex-sources (or vortex-sinks) around the center of the stationary problem, as ε is increased. When $\varepsilon = 0$, we observe the rotation of the point vortex around the neutral equilibrium (the center). When increasing slightly ε , the vortex spirals outwards from its initial position. This is another illustration of the result previously shown (in Fig. 3) : as ε is increased, the neutral point evolves into two repulsive centers. The slow time evolution is an increase of the modulus of C_{11} . Still, our analytical model holds only for weakly nonlinear evolutions and for small ε . The point vortex-source evolution for finite values of ε can only be described numerically. In particular, for $\varepsilon = 0.5$, vortex-sinks leave the vicinity of the neutral point to drift towards the plane center. For large ε ($\varepsilon \geq 0.4$), the point vortex trajectories intersect and the dynamical system becomes irregular. Furthermore, these trajectories are noticeably different for a vortex-source and for a vortex-sink. In the latter case, the trajectory spirals around the plane center.

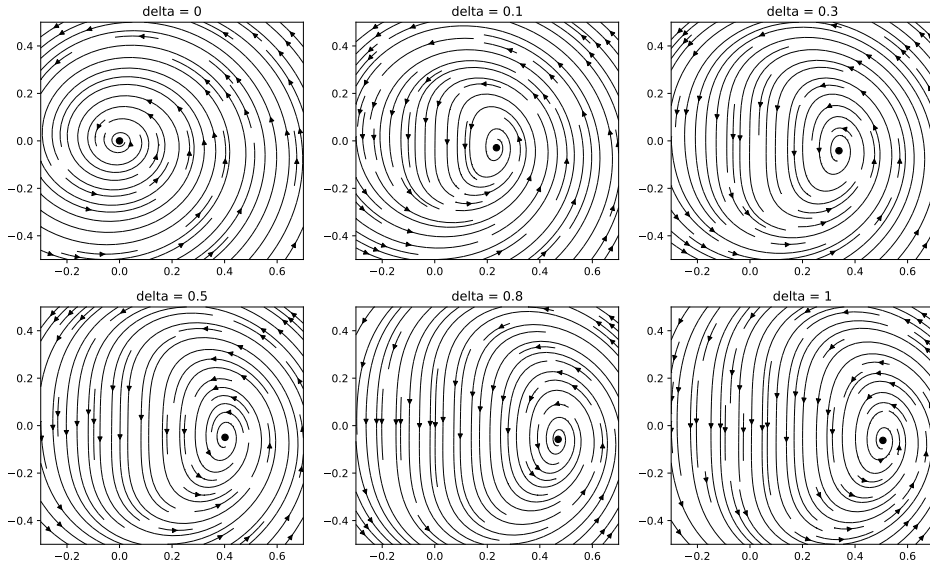


Fig. 5. Slow time evolution of $C_{1,1}(t_2) = X(t_2) + iY(t_2)$ for the harmonic forcing in the case $\omega_2 = 0$ and for $S_0 = -0.01$.

4.2. Passive tracer trajectories

After determining the vortex-source trajectories, we obtain those of passive tracers using also a 4th order Runge Kutta scheme. As a first indication for the possible trajectories of a passive tracer embedded in the time-varying flow, we compute the streamlines of the total flow, for vortex sources at the steady neutral points in Fig. 10. This figure helps position tracers initially. In particular, we see that the topology of the flow is comprised by 6 regions, five of them being compact and symmetric around the plane center, and the external trajectories circling these five regions. These regions enclose five centers and four hyperbolic (saddle) points.

Remark 5. The evolution of a passive tracer (in blue in Figs. 11 and 12) is not that of a vortex-source. The tracer is advected by the two vortex sources simultaneously.

Using Fig. 10, we place passive tracers either near the plane center, or near a neutral point, or in the external region, far away from the plane center, see Figs. 11 and 12. In these figures, the evolution of point vortex-source 1 is plotted in black; this vortex lies initially at the neutral point (which is no more an equilibrium point for $\varepsilon > 0$). For $\varepsilon = 0$, the tracer follows a closed curve around the plane center. For the point-vortex source, we can clearly see that the tracers trajectories move out of the closed regions indicated by Fig. 10 when $\varepsilon = 0.5$. Such a finite amplitude variation of the source strength can be attained when induced by wind variability. It is clear that the tracers is mixed between the various regions. For an oceanographic application, this indicates that finite-area vortices would exchange their water masses in this case.

For a vortex-sink, as mentioned previously, passive particles initially located around a neutral center can drift towards the center of the plane (for $\varepsilon = 0.4$); this indicates that mixing will be even more efficient in this case.

To measure the mixing of the tracers, we compute the trajectories of 100 passive particles initially close to each other and we calculate the time evolution of their RMS (root-mean square) relative distance. Figure 13 shows the motion and the growth in time of a patch of tracers. It indicates that the standard deviation grows initially exponentially fast, with a characteristic time $T=25$. The subsequent growth (at $t=75$) is even faster. A more detailed view of the growth of the patches is provided on Fig. 14. The initial position of the four patches of particles is indicated on Fig. 10. At

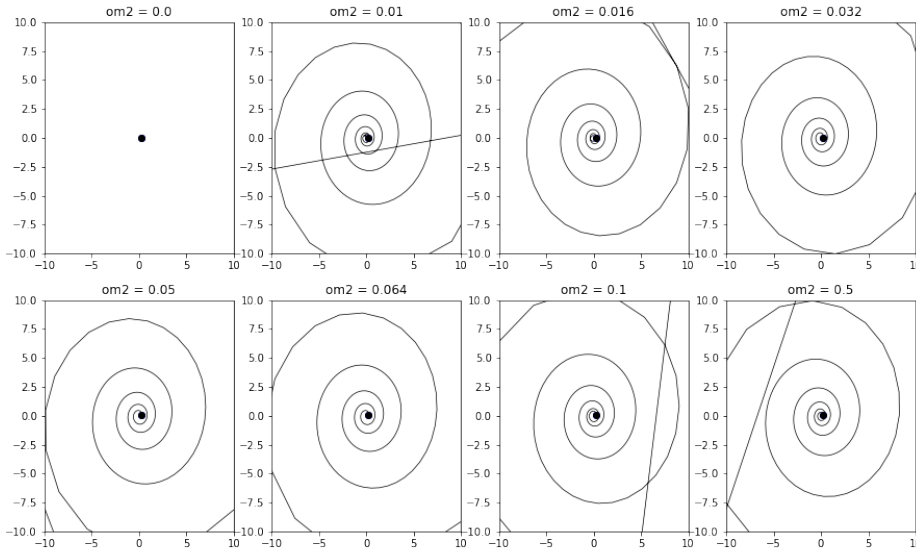


Fig. 6. Trajectories of $C_{1,1}$ for the harmonic forcing in function of ω_2 for $\delta = 0.1$ (then $\tilde{\omega}_2 = 0.016$). The starting point is at the equilibrium point when $\omega_2 = 0$. The source is $S_0 = +0.01$. The straight lines indicate a numerical divergence of the trajectories. The equilibrium point is highly unstable. The calculation time is $T_f = 500$.

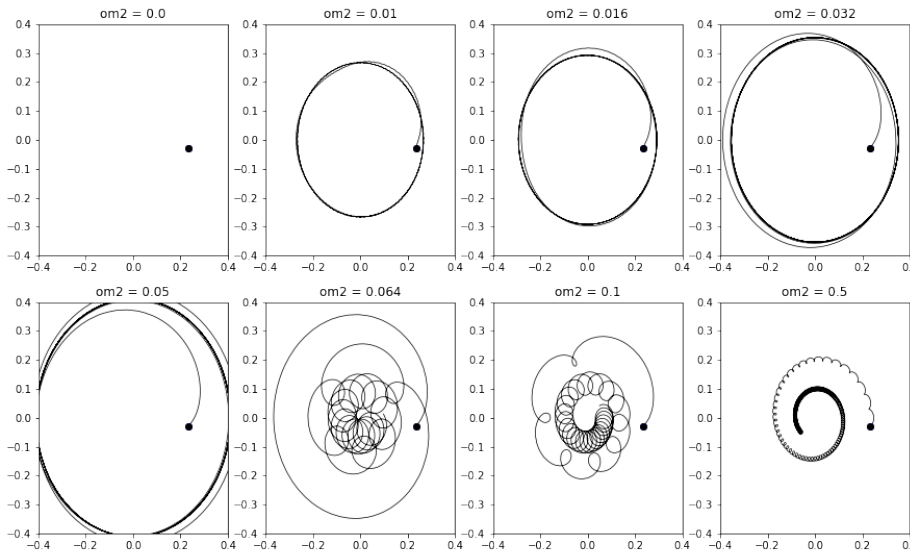


Fig. 7. Trajectories of $C_{1,1}$ for the harmonic forcing in function of ω_2 for $\delta = 0.1$ (then $\tilde{\omega}_2 \sim 0.016$). The starting point is at the equilibrium point when $\omega_2 = 0$. The source is a sink $S_0 = -0.01$ and we can see a stabilisation of $C_{1,1}$ with time. The equilibrium point is stable. The calculation time is $T_f = 2000$. For large ω_2 , it is likely from numerical simulations, that $C_{1,1} \rightarrow 0$ as $t \rightarrow \infty$.

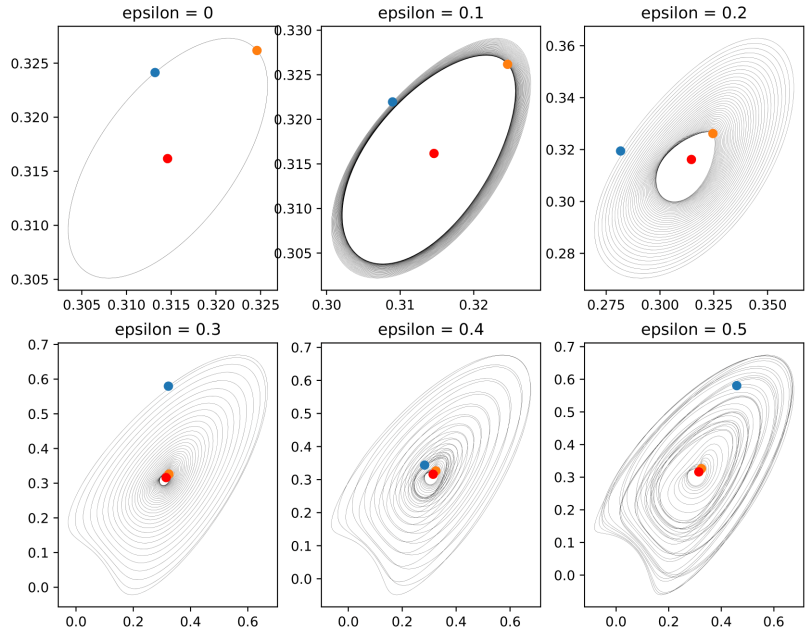


Fig. 8. Trajectories of the vortex-source 1 for $\Gamma_0 = -0.5$, $S_0 = 0.01$, $\Omega = 1$ and $A = 0.8$. The red point is the center equilibrium point, the orange one is the initial position of the vortex and the blue one the position of the vortex at the calculation time $T_f = 300$.

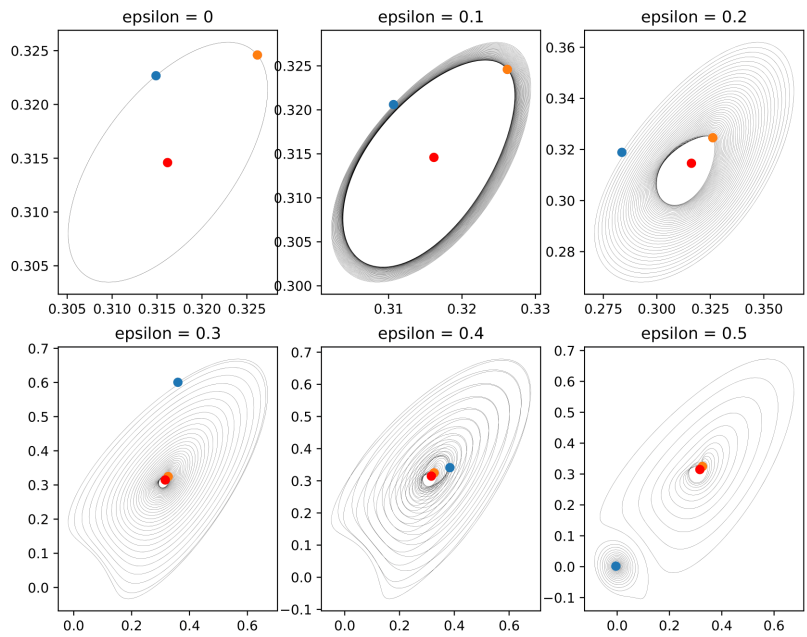


Fig. 9. Trajectories of the vortex-sink 1 for $\Gamma_0 = -0.5$, $S_0 = -0.01$, $\Omega = 1$ and $A = 0.8$. The red point is the center equilibrium point, the orange one is the initial position of the vortex and the blue one the position of the vortex at the calculation time $T_f = 300$.

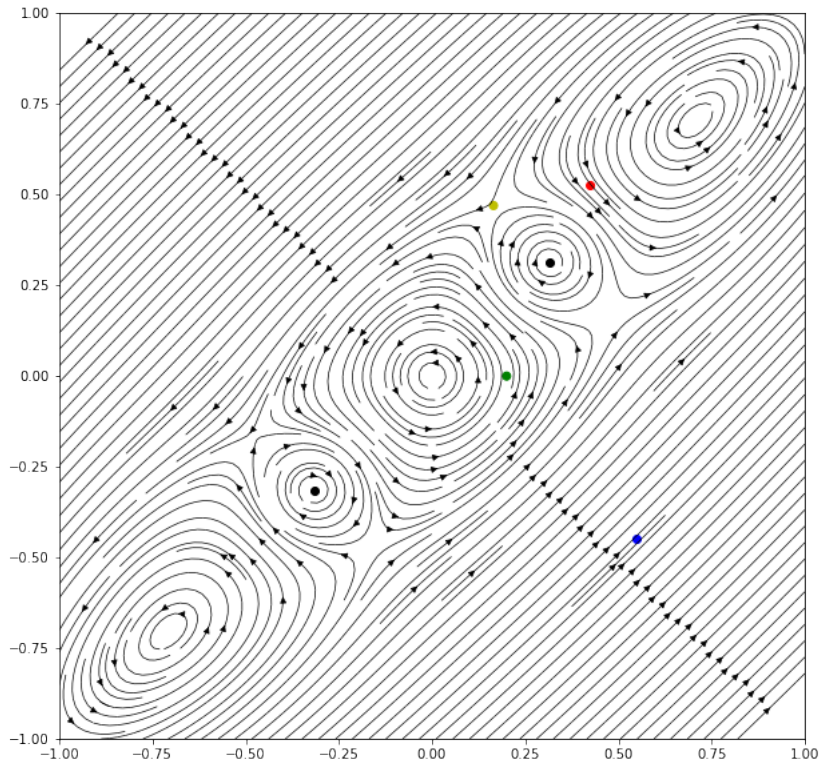


Fig. 10. Streamlines of the total flow when the two vortex-sinks are placed at their equilibrium point (black points), for $\varepsilon = 0$ and for the usual parameters (here we take $S_0 = -0.01$ but it is really similar for the source case). We can see three center equilibrium points (one at the origin and two symmetric), four saddle points and two attractive equilibrium points (the center of the vortex-sinks, they becomes repulsive equilibrium points if we take $S_0 > 0$). The four colored points are the starting points of the patch of tracers we used in the study.

long time, the growth of the tracer patch is similar for $\varepsilon = 0$ and for $\varepsilon = 0.2$ but at shorter time the patch shown on Fig. 13 grows exponentially fast for $\varepsilon = 0.2$.

5. CONCLUSIONS, PERSPECTIVES AND PHYSICAL INTERPRETATIONS

In this paper, we have addressed the problem of two vortex-sources in an external deformation field. Compared with previous studies we have not considered a time-varying external flow but circulation and strength of the source/sink-vortices. We addressed the problem of point vortices analytically. This idealized situation, added to geometrical symmetry in the plane, allows the derivation and analysis of a simple dynamical system. For several values of the physical parameters, we have shown the existence of a center point of equilibrium around which oscillation of the perturbed vortex occurs in a steady configuration.

We then have shown that a periodic variation of circulation or of the source flow, with a sub-harmonic or a harmonic frequency, could be caused by an unsteady wind. With such a variation of Γ or of S , we have calculated the slow evolution of the vortex trajectories from the steady orbit around the center point. The slow variation of the amplitude of the perturbation shows the destabilization of the center point into attractive or repulsive equilibria, for both the harmonic and sub-harmonic variations. The difference between these two cases is the number of equilibria (1 or 2). In both cases, the amplitude of the perturbation in the vicinity of these equilibria is bounded in time for small amplitudes of the time variation of Γ or of S . For larger amplitude variations (larger

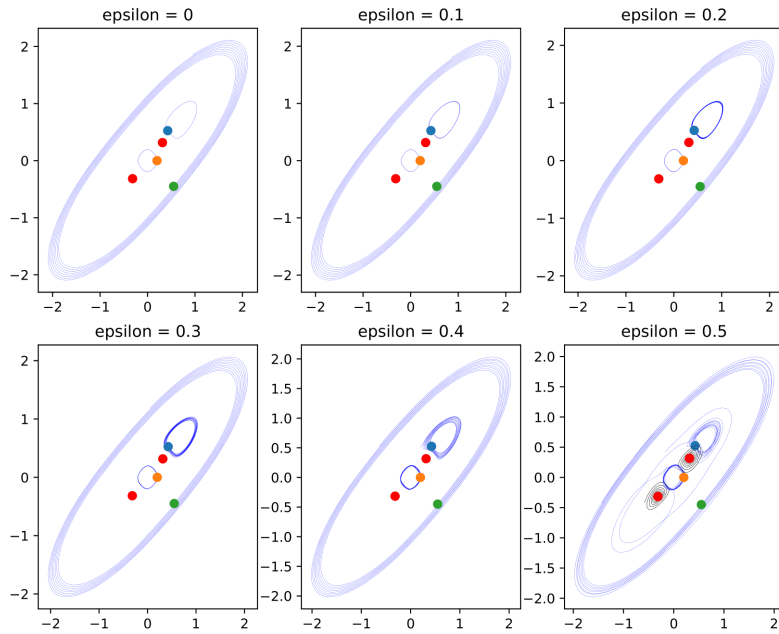


Fig. 11. Tracer evolution in the plane for a vortex-source system as ϵ is increased; in black : vortex-sources trajectory; in blue : passive tracer trajectories. The red points are the initial position of the vortex-sources at their center equilibrium points for $\epsilon = 0$ and the blue, orange and green points are initial positions of the passive tracers. Here the calculation time is $T_f = 100$.

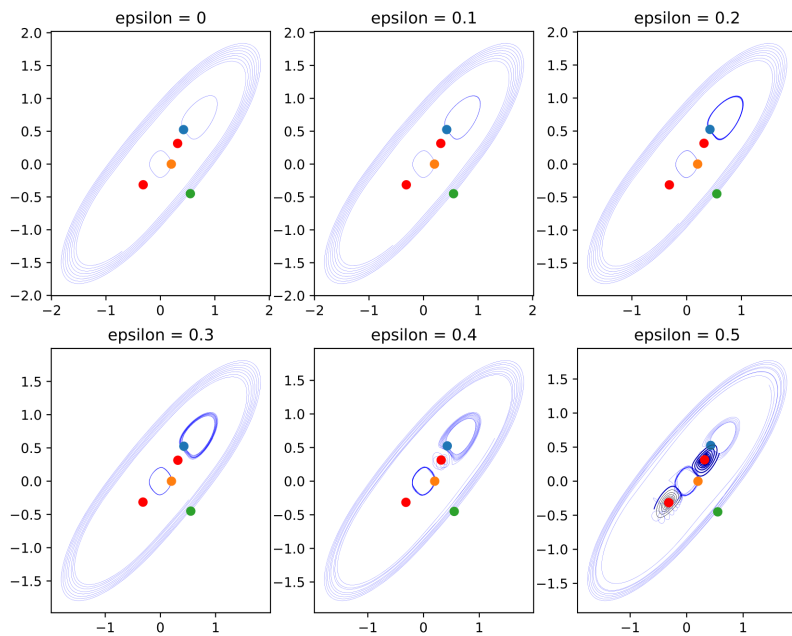


Fig. 12. Tracer evolution in the plane for a vortex-sink system as ϵ is increased. The colors are the same as in Fig. 11 and $T_f = 100$.

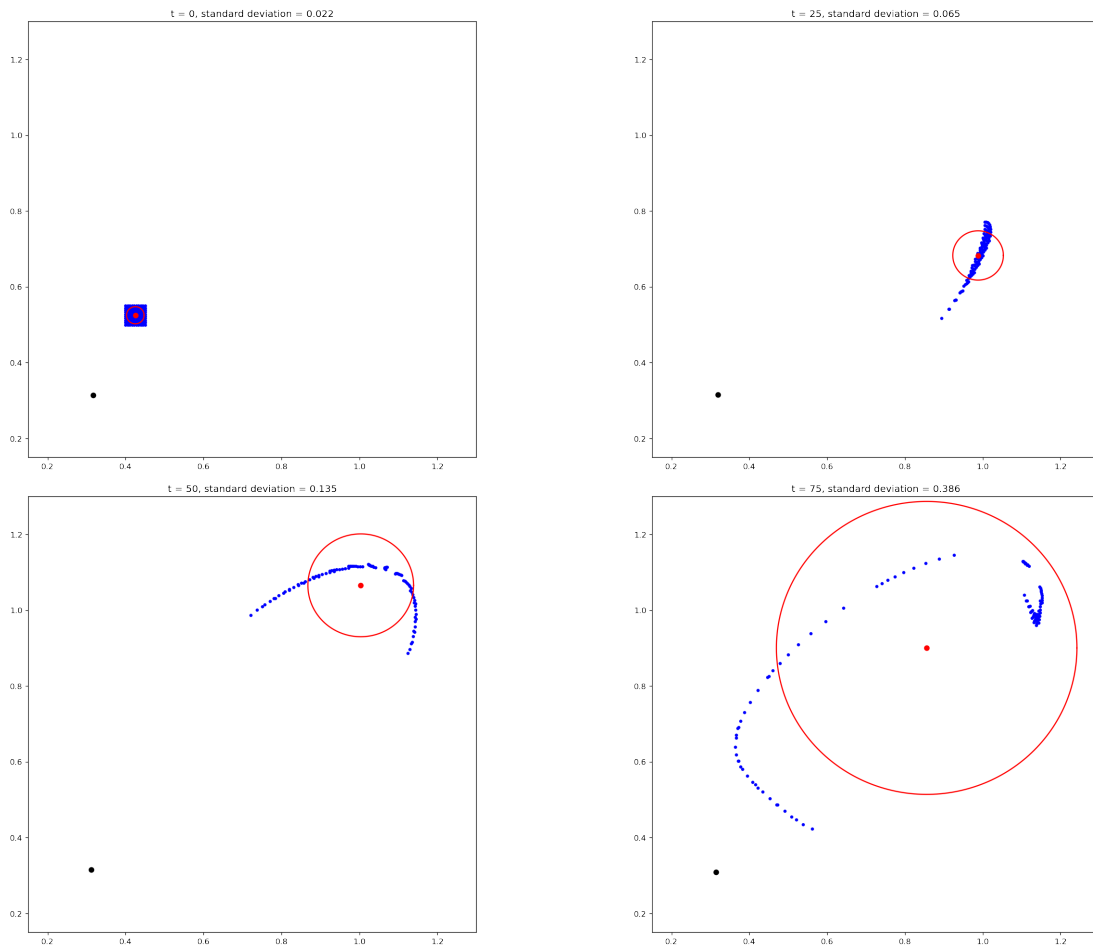


Fig. 13. Evolution of the vortex-sink number 1 (black dot) close to its stable point. Evolution of 100 passive tracers (blue dots), of their global center (red dot) and of the standard deviation of the patch (represented by the red circle). For this experiment, $\varepsilon = 0.2$.

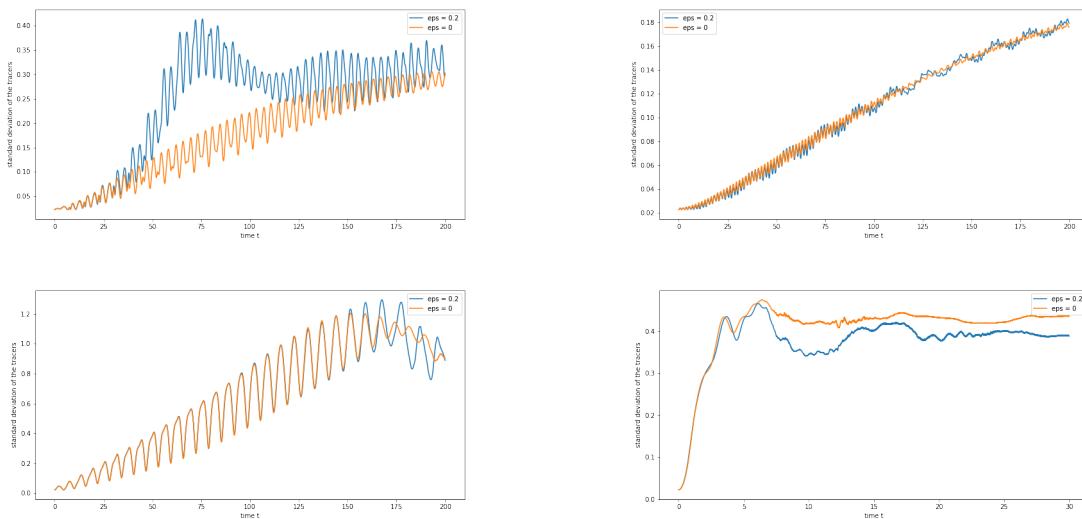


Fig. 14. Evolution of the standard deviation of the patch of tracers for different initial positions (those described in Fig. 10). The last one is for the initial position close to the saddle equilibrium point.

ε), trajectories are allowed between the previous fixed points. This indicates a transition to chaos when ε grows.

We have also computed the evolution and spreading of patches of passive particles. We have shown that the spreading can grow exponentially fast when the time variation of Γ or S is present. This indicates that the effect of an unsteady wind, taken into account via a relative wind stress, can increase the mixing of the fluid (here the oceanic fluid of the two vortices, or in their periphery). From this analysis only, and considering previous studies, it is difficult to predict the exact influence of using the relative wind stress curl to force two interacting finite-area vortices. This will require numerical modelling with a detailed survey in the space of physical parameters as was done by Perrot and Carton [24]. In particular, the orientation of the background flow has been shown to have a crucial importance in facilitating or in reducing the vortex tendency to merge.

The orientation of the wind in our problem is related to the polarity of the source (source or sink) and it would be interesting to study its influence on vortex merger. This can be achieved with a fully coupled ocean-atmosphere quasi-geostrophic model, as a second step of this study. Another important aspect to be studied with a coupled model is the stability of individual, finite-area vortices. Indeed, both vortex interaction which allows their growth (against the ambient shear of the surrounding flows which erode them), and the stability of isolated vortices, are key mechanisms for the durability of these structures. Moreover, they make up the bulk of eddy kinetic energy in the ocean. Understanding eddy kinetic energy variations in coupled ocean-atmosphere models, requires the knowledge of vortex processes in such models.

Ocean-atmosphere coupling create an asymmetric Ekman pumping in the vortex and so the resultant of this pumping is not null and corresponds to a not divergent free flow. The measure of this divergent component is impossible using altimetry because the speed computed from altimetry is geostrophic so divergence free. Surface buoys, ship drifts, or other satellite sensors able to give complete speed are then needed. Future research will compare the total surface velocity field and the one deduced from altimetry and related to wind. This will allow us to better evaluate the impact on the divergence component of the flow on the interactions vortex – vortex.

APPENDIX A. EQUILIBRIUM POINTS AND STABILITY

This section is a reminder of the fixed points of the problem; it was addressed slightly differently in [22] and in [23]. Recall the various cases for equilibria here with our notations and in our specific cases. This is necessary to further study the vortex source evolution with unsteady circulation or source strength.

Recall we have the following condition : $\Gamma_0\Omega < 0$ and formulas :

$$\theta_0 = -\frac{1}{2} \arctan \left[\frac{\Gamma_0 + 4\pi r_0^2 \Omega}{S_0} \right], \quad (\text{A.1})$$

or

$$\theta_0 = -\frac{1}{2} \arctan \left[\frac{\Gamma_0 + 4\pi r_0^2 \Omega}{S_0} \right] + \frac{\pi}{2}, \quad (\text{A.2})$$

and

$$r_0^4(\Omega^2 - A^2) + \frac{\Gamma_0\Omega}{2\pi} r_0^2 + \frac{S_0^2 + \Gamma_0^2}{16\pi^2} = 0. \quad (\text{A.3})$$

1. For $\Omega^2 = A^2$:

Equilibrium Starting from Eq. (A.3) with $\Omega^2 = A^2$ and $\Gamma_0\Omega < 0$, we have $r_0^2 = -\frac{S_0^2 + \Gamma_0^2}{8\pi\Gamma_0\Omega} > 0$ and thanks to Eq. (A.1), we have

$$r_0 = \sqrt{\frac{S_0^2 + \Gamma_0^2}{8\pi(-\Gamma_0\Omega)}} \quad \text{and} \quad \theta_0 = \frac{1}{2} \arctan \left[\frac{S_0^2 - \Gamma_0^2}{2S_0\Gamma_0} \right]. \quad (\text{A.4})$$

Stability Is the equilibrium (A.4) stable ? From the characteristic polynomial (2.7) of the differential matrix $\chi(X) = X^2 - \frac{S_0^2 + \Gamma_0^2 + 4\pi r_0^2 \Gamma_0 \Omega}{4\pi^2 r_0^4}$, we need to determine the sign of Δ_0 :

$$\Delta_0 = S_0^2 + \Gamma_0^2 + 4\pi r_0^2 \Gamma_0 \Omega = \frac{S_0^2 + \Gamma_0^2}{2} > 0. \quad (\text{A.5})$$

So χ has two real roots : one positive and one negative. Then the equilibrium (A.4) is a saddle equilibrium point. We are not interested in this type of equilibrium.

2. For $\Omega^2 \neq A^2$:

From the polynomial equation Eq. (A.3) in r_0^2 :

$$(\Omega^2 - A^2) X^2 + \frac{\Gamma_0 \Omega}{2\pi} X + \frac{S_0^2 + \Gamma_0^2}{16\pi^2} = 0, \quad (\text{A.6})$$

we compute the discriminant

$$\Delta = \frac{1}{4\pi^2} [\Gamma_0^2 \Omega^2 - (S_0^2 + \Gamma_0^2) (\Omega^2 - A^2)], \quad (\text{A.7})$$

and look at the sign of

$$\Delta' = A^2 (S_0^2 + \Gamma_0^2) - S_0^2 \Omega^2, \quad (\text{A.8})$$

$$\Delta' = S_0^2 (A^2 - \Omega^2) + A^2 \Gamma_0^2. \quad (\text{A.9})$$

We want Δ' to be positive because we want real (positive) solutions to Eq. (A.6). This brings three situations (we have already study the situation $\Omega^2 = A^2$) :

- If $A^2 > \Omega^2$, then $\Delta' > 0$ clearly from Eq. (A.9).
- If $\Omega^2 > A^2$, then $\Delta' > 0 \iff \Omega^2 < A^2 \left(1 + \frac{\Gamma_0^2}{S_0^2}\right)$.
- If $\Omega^2 = A^2 \left(1 + \frac{\Gamma_0^2}{S_0^2}\right)$, then $\Delta' = 0$.

a. For $A^2 > \Omega^2$:

Because $A^2 > \Omega^2$, we have $\Delta' > 0$ without any more condition, and we have two solutions to the polynomial equation Eq. (A.6) :

$$X_{\pm} = \frac{\Gamma_0 \Omega \pm \sqrt{\Delta'}}{4\pi (A^2 - \Omega^2)}. \quad (\text{A.10})$$

Recall we want only non-negative solution ($r_0^2 > 0$). Because we have supposed the condition $\Gamma_0 \Omega < 0$, this constraint removes X_- . The root X_+ is a non-negative solution if and only if $\sqrt{\Delta'} > -\Gamma_0 \Omega > 0$. This condition is valid because $(A^2 - \Omega^2) (S_0^2 + \Gamma_0^2) > 0$ so $\Delta' > \Gamma_0^2 \Omega^2$.

Equilibrium for X_+ We have the following equilibrium point (with θ_0 computed from Eq. (A.1)) :

$$r_0 = \sqrt{\frac{\Gamma_0 \Omega + \sqrt{\Delta'}}{4\pi (A^2 - \Omega^2)}} \quad \text{and} \quad \theta_0 = -\frac{1}{2} \arctan \left[\frac{\Gamma_0 A^2 + \Omega \sqrt{\Delta'}}{S_0 (A^2 - \Omega^2)} \right]. \quad (\text{A.11})$$

Stability for X_+ How the equilibrium (A.11) is stable ? We need to know the sign of Δ_0 .

Proposition 1. *Under all the conditions of this subsection, we have*

$$\Delta_0 = S_0^2 + \Gamma_0^2 + 4\pi r_0^2 \Gamma_0 \Omega > 0$$

and the equilibrium point (A.11) is a saddle equilibrium point.

Proof. Remember we work under the assumption $A^2 > \Omega^2$ and $\Gamma_0 \Omega < 0$. Then, put r_0^2 in Δ_0 and :

$$\begin{aligned} \Delta_0 > 0 &\iff (S_0^2 + \Gamma_0^2) (A^2 - \Omega^2) + \Gamma_0^2 \Omega^2 > -\Gamma_0 \Omega \sqrt{\Delta'} \\ &\iff [S_0^2 (A^2 - \Omega^2) + \Gamma_0^2 A^2]^2 > \Gamma_0^2 \Omega^2 S_0^2 (A^2 - \Omega^2) + \Gamma_0^4 \Omega^2 A^2 \\ &\iff S_0^4 (A^2 - \Omega^2) + S_0^2 \Gamma_0^2 (2A^2 - \Omega^2) + \Gamma_0^4 A^2 > 0 \end{aligned}$$

The right hand side of the equivalence is true under the assumption $A^2 > \Omega^2$. This conclude the proof of the proposition.

$$b. \text{ For } A^2 < \Omega^2 < A^2 \left(1 + \frac{\Gamma_0^2}{S_0^2}\right) :$$

We also have two roots of the polynomial (A.6) :

$$X_{\pm} = \frac{-\Gamma_0 \Omega \pm \sqrt{\Delta'}}{4\pi (\Omega^2 - A^2)}. \quad (\text{A.12})$$

X_+ is clearly non-negative. X_- is also non-negative because we have $-\Gamma_0 \Omega > \sqrt{\Delta'} > 0$ (deduced from the hypothesis). So we have two situations to analyse :

Equilibrium and stability for X_+ We have the following equilibrium point (with θ_0 computed from Eq. (A.1)) :

$$r_0 = \sqrt{\frac{-\Gamma_0 \Omega + \sqrt{\Delta'}}{4\pi (\Omega^2 - A^2)}} \quad \text{and} \quad \theta_0 = \frac{1}{2} \arctan \left[\frac{\Gamma_0 A^2 - \Omega \sqrt{\Delta'}}{S_0 (\Omega^2 - A^2)} \right]. \quad (\text{A.13})$$

How this equilibrium (A.13) is stable ? We need to know the sign of Δ_0 .

Proposition 2. *Whatever the set of parameters we choose, if they satisfy the assumptions we made : $A^2 < \Omega^2 < A^2 \left(1 + \frac{\Gamma_0^2}{S_0^2}\right)$ and $\Gamma_0 \Omega < 0$, then we have*

$$\Delta_0 = S_0^2 + \Gamma_0^2 + 4\pi r_0^2 \Gamma_0 \Omega < 0, \quad (\text{A.14})$$

and the equilibrium point (A.13) is a neutral equilibrium point.

Proof. Consider Δ_0 for the value r_0 we have in Eq. (A.13) :

$$\Delta_0 = S_0^2 + \Gamma_0^2 + \Gamma_0 \Omega \left(\frac{-\Gamma_0 \Omega + \sqrt{\Delta'}}{\Omega^2 - A^2} \right).$$

So

$$\begin{aligned} \Delta_0 < 0 &\iff (S_0^2 + \Gamma_0^2) (\Omega^2 - A^2) - \Gamma_0^2 \Omega^2 + \Gamma_0 \Omega \sqrt{\Delta'} < 0 \\ &\iff S_0^2 (\Omega^2 - A^2) + \Gamma_0^2 A^2 + \Gamma_0 \Omega \sqrt{\Delta'} < 0. \end{aligned}$$

The right hand side of the equivalence is true because $\Gamma_0 \Omega < 0$ and $\Omega^2 - A^2 < A^2 \frac{\Gamma_0^2}{S_0^2}$ so $S_0^2 (\Omega^2 - A^2) + \Gamma_0^2 A^2 < 0$. This conclude the proof of the proposition.

Equilibrium and stability for X_- We have the following equilibrium point (with θ_0 computed from Eq. (A.1)) :

$$r_0 = \sqrt{\frac{-\Gamma_0\Omega - \sqrt{\Delta'}}{4\pi(\Omega^2 - A^2)}} \quad \text{and} \quad \theta_0 = \frac{1}{2} \arctan \left[\frac{\Gamma_0 A^2 + \Omega\sqrt{\Delta'}}{S_0(\Omega^2 - A^2)} \right]. \quad (\text{A.15})$$

Proposition 3. *For the equilibrium (A.15), Δ_0 is non-negative for every set of parameters such that $A^2 < \Omega^2 < A^2 \left(1 + \frac{\Gamma_0^2}{S_0^2}\right)$ and $\Gamma_0\Omega < 0$. So the equilibrium (A.15) is a saddle equilibrium point.*

Proof. Look at the expression of Δ_0 :

$$\Delta_0 = S_0^2 + \Gamma_0^2 + 4\pi r_0^2 \Gamma_0 \Omega = S_0^2 + \Gamma_0^2 + \frac{-\Gamma_0^2 \Omega^2 - \Gamma_0 \Omega \sqrt{\Delta'}}{\Omega^2 - A^2}, \quad (\text{A.16})$$

which the sign is the same as the sign of

$$(S_0^2 + \Gamma_0^2)(\Omega^2 - A^2) - \Gamma_0^2 \Omega^2 - \Gamma_0 \Omega \sqrt{\Delta'} = \underbrace{S_0^2(\Omega^2 - A^2) - \Gamma_0^2 A^2}_{<0 \text{ because } \Omega^2 - A^2 < A^2 \frac{\Gamma_0^2}{S_0^2}} + \underbrace{(-\Gamma_0 \Omega \sqrt{\Delta'})}_{>0} \quad (\text{A.17})$$

So we have the following equivalences :

$$\begin{aligned} \Delta_0 > 0 &\iff -\Gamma_0 \Omega \sqrt{\Delta'} > \Gamma_0^2 A^2 - S_0^2 (\Omega^2 - A^2) \\ &\iff \Gamma_0^2 \Omega^2 \Delta' > (\Gamma_0^2 A^2 - S_0^2 (\Omega^2 - A^2))^2 \\ &\iff \Gamma_0^2 \Omega^2 S_0^2 (A^2 - \Omega^2) + \Gamma_0^4 A^2 (\Omega^2 - A^2) > -2\Gamma_0^2 A^2 S_0^2 (\Omega^2 - A^2) + S_0^4 (\Omega^2 - A^2)^2 \\ &\iff S_0^4 (\Omega^2 - A^2) + S_0^2 \Gamma_0^2 (\Omega^2 - 2A^2) - \Gamma_0^4 A^2 < 0. \end{aligned}$$

We have to study the sign of a second degree polynomial in S_0^2 for which the discriminant is

$$\delta = \Gamma_0^4 (\Omega^2 - 2A^2)^2 + 4\Gamma_0^4 A^2 (\Omega^2 - A^2) = \Gamma_0^4 \Omega^4 > 0. \quad (\text{A.18})$$

The two roots are

$$\frac{-\Gamma_0^2 (\Omega^2 - 2A^2) + \Gamma_0^2 \Omega^2}{2(\Omega^2 - A^2)} = \frac{A^2 \Gamma_0^2}{\Omega^2 - A^2} > 0, \quad (\text{A.19})$$

and

$$\frac{-\Gamma_0^2 (\Omega^2 - 2A^2) - \Gamma_0^2 \Omega^2}{2(\Omega^2 - A^2)} = -\Gamma_0^2 < 0. \quad (\text{A.20})$$

Because $S_0^2 > 0$, to have $\Delta_0 > 0$, we need S_0^2 to be smaller than the largest root, but this is not an additional constraint because :

$$\begin{aligned} S_0^2 < \frac{A^2 \Gamma_0^2}{\Omega^2 - A^2} &\iff (\Omega^2 - A^2) S_0^2 < A^2 \Gamma_0^2 \\ &\iff \Omega^2 < A^2 \left(1 + \frac{\Gamma_0^2}{S_0^2}\right). \end{aligned}$$

So the polynomial $(\Omega^2 - A^2) X^2 + \Gamma_0^2 (\Omega^2 - 2A^2) X - \Gamma_0^4 A^2$ is non-positive for every values between 0 and $\frac{A^2 \Gamma_0^2}{\Omega^2 - A^2}$. Because S_0^2 is in this interval, we have $\Delta_0 > 0$ for every set of parameters such that $A^2 < \Omega^2 < A^2 \left(1 + \frac{\Gamma_0^2}{S_0^2}\right)$ and $\Gamma_0\Omega < 0$.

$$c. \text{ For } \Omega^2 = A^2 \left(1 + \frac{\Gamma_0^2}{S_0^2}\right)$$

In this section, we have $\Delta' = 0$. Then there is only one solution of Eq. (A.6) :

$$X = \frac{-\Gamma_0\Omega}{4\pi(\Omega^2 - A^2)} = \frac{\Gamma_0^2 + S_0^2}{4\pi(-\Gamma_0\Omega)} > 0. \quad (\text{A.21})$$

This gives the following equilibrium point :

$$r_0 = \sqrt{\frac{\Gamma_0^2 + S_0^2}{4\pi(-\Gamma_0\Omega)}} \quad \text{and} \quad \theta_0 = \frac{1}{2} \arctan\left(\frac{S_0}{\Gamma_0}\right). \quad (\text{A.22})$$

To know the type of stability, we compute Δ_0 :

$$\Delta_0 = S_0^2 + \Gamma_0^2 + 4\pi r_0^2 \Gamma_0 \Omega = S_0^2 + \Gamma_0^2 + \Gamma_0 \Omega \frac{\Gamma_0^2 + S_0^2}{(-\Gamma_0\Omega)} = 0. \quad (\text{A.23})$$

So we cannot conclude about the stability of the equilibrium (A.22).

APPENDIX B. MULTIPLE TIME SCALE DEVELOPMENT

The multiple time scale method is here expanded for the subharmonic case. The harmonic case is similar.

1. Order ε^1

We have the following system at order ε^1 , computed from Eqs. (3.5) and (3.8) :

$$\begin{cases} \partial_{t_0} r_1 = -ar_1 - b(r_0\theta_1) \\ \partial_{t_0} (r_0\theta_1) = -cr_1 + a(r_0\theta_1) \end{cases} \quad (\text{B.1})$$

So

$$\begin{cases} r_1 = C_{1,1}(t_2, t_3) e^{i\omega_0 t_0} + \text{c. c} \\ r_0\theta_1 = D_{1,1}(t_2, t_3) e^{i\omega_0 t_0} + \text{c. c} \end{cases} \quad (\text{B.2})$$

with

$$D_{1,1}(t_2, t_3) = \mu_1 C_{1,1}(t_2, t_3), \quad (\text{B.3})$$

and $\mu_1 = -\frac{a+i\omega_0}{b}$.

2. Order ε^2

With Eqs. (3.6) and (3.9) and because $\partial_{t_1} r_1 = \partial_{t_1} (r_0\theta_1) = 0$, we have the following system in $(r_2, r_0\theta_2)$:

$$\begin{cases} \partial_{t_0} r_2 = -ar_2 - b(r_0\theta_2) + f_2(t_0, t_1, t_2, t_3) \\ \partial_{t_0} (r_0\theta_2) = -cr_2 + a(r_0\theta_2) + g_2(t_0, t_1, t_2, t_3) \end{cases} \quad (\text{B.4})$$

where :

$$\begin{cases} f_2(t_0, t_1, t_2, t_3) = \frac{a\delta r_0}{2} \cos(2\omega_0 t_0) + \frac{a}{2r_0} r_1^2 + \frac{a}{r_0} (r_0\theta_1)^2 - \frac{b}{r_0} r_1 (r_0\theta_1) \\ g_2(t_0, t_1, t_2, t_3) = \frac{c\delta r_0}{2} \cos(2\omega_0 t_0) + \frac{3c}{2r_0} r_1^2 + \frac{b}{r_0} (r_0\theta_1)^2 \end{cases} \quad (\text{B.5})$$

The system (B.4) gives :

- For r_2 :

$$\begin{aligned}\partial_{t_0}^2 r_2 &= -a(-ar_2 - b(r_0\theta_2) + f_2) - b(-cr_2 + a(r_0\theta_2) + g_2) + \partial_{t_0} f_2 \\ &= (a^2 + bc) r_2 + h_2(t_0, t_1, t_2, t_3).\end{aligned}\quad (\text{B.6})$$

- For $r_0\theta_2$:

$$\begin{aligned}\partial_{t_0}^2 (r_0\theta_2) &= -c(-ar_2 - b(r_0\theta_2) + f_2) + a(-cr_2 + a(r_0\theta_2) + g_2) + \partial_{t_0} g_2 \\ &= (bc + a^2) (r_0\theta_2) + k_2(t_0, t_1, t_2, t_3).\end{aligned}\quad (\text{B.7})$$

where :

$$\begin{cases} h_2(t_0, t_1, t_2, t_3) = (-af_2 - bg_2 + \partial_{t_0} f_2) (t_0, t_1, t_2, t_3) \\ k_2(t_0, t_1, t_2, t_3) = (-cf_2 + ag_2 + \partial_{t_0} g_2) (t_0, t_1, t_2, t_3) \end{cases}\quad (\text{B.8})$$

- Development of f_2 :

$$\begin{aligned}f_2 &= \frac{a}{r_0} \left[3 - \frac{2c}{b} \right] |C_{1,1}|^2 \\ &\quad + \left[\frac{ar_0}{4} + \frac{C_{1,1}^2}{r_0} \left(\frac{3a}{2} + \frac{a(a+i\omega_0)^2}{b^2} + i\omega_0 \right) \right] e^{2i\omega_0 t_0} + \text{c. c} \\ f_2 &= F_{2,0}|C_{1,1}|^2 + [F_{2,2,1} + F_{2,2,2}C_{1,1}^2] e^{2i\omega_0 t_0} + \text{c. c}.\end{aligned}\quad (\text{B.9})$$

- Development of g_2 :

$$\begin{aligned}g_2 &= \frac{c}{r_0} |C_{1,1}|^2 + \left[\frac{cr_0}{4} + \frac{C_{1,1}^2}{r_0} \left(\frac{3c}{2} + \frac{(a+i\omega_0)^2}{b} \right) \right] e^{2i\omega_0 t_0} + \text{c. c} \\ g_2 &= G_{2,0}|C_{1,1}|^2 + [G_{2,2,1} + G_{2,2,2}C_{1,1}^2] e^{2i\omega_0 t_0} + \text{c. c}.\end{aligned}\quad (\text{B.10})$$

- Development of h_2 :

$$\begin{aligned}h_2 &= [-aF_{2,0} - bG_{2,0}] |C_{1,1}|^2 + [(-bG_{2,2,1} + (-a + 2i\omega_0) F_{2,2,1}) \\ &\quad + (-bG_{2,2,2} + (-a + 2i\omega_0) F_{2,2,2}) C_{1,1}^2] e^{2i\omega_0 t_0} + \text{c. c} \\ h_2 &= H_{2,0}|C_{1,1}|^2 + [H_{2,2,1} + H_{2,2,2}C_{1,1}^2] e^{2i\omega_0 t_0} + \text{c. c}.\end{aligned}\quad (\text{B.11})$$

- Development of k_2 :

$$\begin{aligned}k_2 &= [-cF_{2,0} + aG_{2,0}] |C_{1,1}|^2 + [(-cF_{2,2,1} + (a + 2i\omega_0) G_{2,2,1}) \\ &\quad + (-cF_{2,2,2} + (a + 2i\omega_0) G_{2,2,2}) C_{1,1}^2] e^{2i\omega_0 t_0} + \text{c. c} \\ k_2 &= K_{2,0}|C_{1,1}|^2 + [K_{2,2,1} + K_{2,2,2}C_{1,1}^2] e^{2i\omega_0 t_0} + \text{c. c}.\end{aligned}\quad (\text{B.12})$$

Then from Eqs. (B.6) and (B.7), we have

- The homogeneous solutions :

$$\begin{cases} r_2 = C_{2,1} e^{i\omega_0 t_0} + \text{c. c} \\ (r_0\theta_2) = D_{2,1} e^{i\omega_0 t_0} + \text{c. c} \end{cases}\quad (\text{B.13})$$

- The particular solutions for the constant terms :

$$\begin{cases} r_2 = \frac{H_{2,0}}{\omega_0^2} |C_{1,1}|^2 \\ (r_0\theta_2) = \frac{K_{2,0}}{\omega_0^2} |C_{1,1}|^2 \end{cases} \quad (\text{B.14})$$

- The particular solutions for $e^{2i\omega_0 t_0} + \text{c. c}$:

$$\begin{cases} r_2 = -\frac{H_{2,2,1} + H_{2,2,2} C_{1,1}^2}{3\omega_0^2} e^{2i\omega_0 t_0} + \text{c. c} \\ (r_0\theta_2) = -\frac{K_{2,2,1} + K_{2,2,2} C_{1,1}^2}{3\omega_0^2} e^{2i\omega_0 t_0} + \text{c. c} \end{cases} \quad (\text{B.15})$$

So the total solution of Eqs. (B.6) and (B.7) is :

$$\begin{cases} r_2 = C_{2,0} |C_{1,1}|^2 + C_{2,1} e^{i\omega_0 t_0} + \text{c. c} + (C_{2,2,1} + C_{2,2,2} C_{1,1}^2) e^{2i\omega_0 t_0} + \text{c. c} \\ (r_0\theta_2) = D_{2,0} |C_{1,1}|^2 + D_{2,1} e^{i\omega_0 t_0} + \text{c. c} + (D_{2,2,1} + D_{2,2,2} C_{1,1}^2) e^{2i\omega_0 t_0} + \text{c. c} \end{cases} \quad (\text{B.16})$$

with (for $i = 1, 2$)

$$C_{2,0} = \frac{H_{2,0}}{\omega_0^2}, \quad C_{2,2,i} = -\frac{H_{2,2,i}}{3\omega_0^2}, \quad D_{2,0} = \frac{K_{2,0}}{\omega_0^2}, \quad D_{2,2,i} = -\frac{K_{2,2,i}}{3\omega_0^2}. \quad (\text{B.17})$$

3. Order ε^3

With Eqs. (3.7) and (3.10), we have the following system at the order ε^3 :

$$\begin{cases} \partial_{t_0} r_3 = -ar_3 - b(r_0\theta_3) + f_3(t_0, t_1, t_2, t_3) \\ \partial_{t_0} (r_0\theta_3) = -cr_3 + a(r_0\theta_3) + g_3(t_0, t_1, t_2, t_3) \end{cases} \quad (\text{B.18})$$

where f_3 and g_3 are the following given functions :

$$\begin{cases} f_3 = -\partial_{t_2} r_1 + \frac{ar_1 r_2}{r_0} - \frac{ar_1^3}{2r_0^2} - \frac{ar_1 \cos(2\omega_0 t_0)}{2} - \frac{b(r_2(r_0\theta_1) + r_1(r_0\theta_2))}{r_0} + \frac{ar_1(r_0\theta_1)^2}{r_0^2} \\ \quad + \frac{2a(r_0\theta_1)(r_0\theta_2)}{r_0} + \frac{2b(r_0\theta_1)^3}{3r_0^2} - ar_0\omega_0 t_1 \sin(2\omega_0 t_0) \\ g_3 = -\partial_{t_2} (r_0\theta_1) + \frac{3cr_1 r_2}{r_0} - \frac{2cr_1^3}{r_0^2} - cr_1 \cos(2\omega_0 t_0) - \frac{2a(r_0\theta_1)^3}{3r_0^2} + \frac{2b(r_0\theta_1)(r_0\theta_2)}{r_0} \\ \quad - c\omega_0 t_1 \sin(2\omega_0 t_0) \end{cases} \quad (\text{B.19})$$

The system (B.18) gives :

- For r_3 :

$$\begin{aligned} \partial_{t_0}^2 r_3 &= -a(-ar_3 - b(r_0\theta_3) + f_3) - b(-cr_3 + a(r_0\theta_3) + g_3) + \partial_{t_0} f_3 \\ &= (a^2 + bc) r_3 + h_3. \end{aligned} \quad (\text{B.20})$$

- For $r_0\theta_3$:

$$\begin{aligned} \partial_{t_0}^2 (r_0\theta_3) &= -c(-ar_3 - b(r_0\theta_3) + f_3) + a(-cr_3 + a(r_0\theta_3) + g_3) + \partial_{t_0} g_3 \\ &= (bc + a^2) (r_0\theta_3) + k_3. \end{aligned} \quad (\text{B.21})$$

We do not develop f_3 , g_3 , h_3 and k_3 like we did for the order ε^2 . We only introduce the following notations :

$$\begin{cases} f_3 = F_{3,0} + F_{3,1} e^{i\omega_0 t_0} + F_{3,2} e^{2i\omega_0 t_0} + F_{3,3} e^{3i\omega_0 t_0} + \text{c. c} \\ g_3 = G_{3,0} + G_{3,1} e^{i\omega_0 t_0} + G_{3,2} e^{2i\omega_0 t_0} + G_{3,3} e^{3i\omega_0 t_0} + \text{c. c} \\ h_3 = H_{3,0} + H_{3,1} e^{i\omega_0 t_0} + H_{3,2} e^{2i\omega_0 t_0} + H_{3,3} e^{3i\omega_0 t_0} + \text{c. c} \\ k_3 = K_{3,0} + K_{3,1} e^{i\omega_0 t_0} + K_{3,2} e^{2i\omega_0 t_0} + K_{3,3} e^{3i\omega_0 t_0} + \text{c. c} \end{cases} \quad (\text{B.22})$$

Then if we denote by L the self-adjoint linear operator $\partial_{t_0}^2 + \omega_0^2$, we have $r_1^* L r_3 = r_1^* h_3 = r_1^* L^* r_3 = 0 = \langle r_1, h_3 \rangle$. But $\langle e^{in\omega_0 t_0}, e^{ip\omega_0 t_0} \rangle = \delta_{n,p}$ (Kronecker symbol) for $n, p \in \mathbf{Z}$ and because $r_1 = C_{1,1} e^{i\omega_0 t_0} + \text{c. c}$, we have

$$\langle r_1, h_3 \rangle = C_{1,1} H_{3,1} + \text{c. c} = 0. \quad (\text{B.23})$$

Because $H_{3,1} = (-a + i\omega_0)F_{3,1} - bG_{3,1}$, we deduce the amplitude equation :

$$(-a + i\omega_0)F_{3,1} - bG_{3,1} = 0. \quad (\text{B.24})$$

So we only have to compute $F_{3,1}$ and $G_{3,1}$ from Eq. (B.19) : writing

$$\begin{cases} F_{3,1} = -\partial_{t_2} C_{1,1} + \text{I} \overline{C_{1,1}} + \text{II} |C_{1,1}|^2 C_{1,1} \\ G_{3,1} = \frac{a+i\omega_0}{b} \partial_{t_2} C_{1,1} + \text{III} \overline{C_{1,1}} + \text{IV} |C_{1,1}|^2 C_{1,1} \end{cases} \quad (\text{B.25})$$

we have :

$$\text{I} = -\frac{a}{4} + \frac{C_{2,2,1}}{r_0} (2a - i\omega_0) + \frac{D_{2,2,1}}{r_0} \left(-b - \frac{2a^2}{b} + \frac{2ai\omega_0}{b} \right), \quad (\text{B.26})$$

$$\begin{aligned} \text{II} = & \frac{1}{r_0^2} \left[a \left(-\frac{3}{2} + 2\frac{a^2}{b^2} + \frac{c}{b} \right) + 2i\omega_0 \left(\frac{a^2}{b^2} + \frac{c}{b} \right) \right] \\ & + \frac{C_{2,0}}{r_0} (2a + i\omega_0) + \frac{D_{2,0}}{r_0} \left(-b - \frac{2a^2}{b} - \frac{2ai\omega_0}{b} \right) \\ & + \frac{C_{2,2,2}}{r_0} (2a - i\omega_0) + \frac{D_{2,2,2}}{r_0} \left(-b - \frac{2a^2}{b} + \frac{2ai\omega_0}{b} \right), \end{aligned} \quad (\text{B.27})$$

$$\text{III} = -\frac{c}{2} + \frac{3c}{r_0} C_{2,2,1} + \frac{2D_{2,2,1}}{r_0} (-a + i\omega_0), \quad (\text{B.28})$$

$$\begin{aligned} \text{IV} = & -\frac{6c}{r_0^2} - \frac{2ac}{r_0^2 b^2} (a + i\omega_0) + \frac{3c}{r_0} (C_{2,0} + C_{2,2,2}) \\ & - \frac{2}{r_0} ((a + i\omega_0) D_{2,0} + (a - i\omega_0) D_{2,2,2}). \end{aligned} \quad (\text{B.29})$$

From Eq. (B.24) we obtain the amplitude equation

$$\partial_{t_2} C_{1,1} = (\text{V} + i\text{VI}) \overline{C_{1,1}} + (\text{VII} + i\text{VIII}) |C_{1,1}|^2 C_{1,1}, \quad (\text{B.30})$$

with

$$\begin{cases} \text{V} = \text{Re} \left(-\frac{(a-i\omega_0)\text{I}+b\text{III}}{2i\omega_0} \right) \\ \text{VI} = \text{Im} \left(-\frac{(a-i\omega_0)\text{I}+b\text{III}}{2i\omega_0} \right) \\ \text{VII} = \text{Re} \left(-\frac{(a-i\omega_0)\text{II}+b\text{IV}}{2i\omega_0} \right) \\ \text{VIII} = \text{Im} \left(-\frac{(a-i\omega_0)\text{II}+b\text{IV}}{2i\omega_0} \right) \end{cases} \quad (\text{B.31})$$

ACKNOWLEDGMENTS

The first author thanks Ecole Normale Supérieure de Rennes (Maths Department) for a Ph.D. grant allowing the completion of this work.

The authors thank Dr Jean N. Reinaud for proof reading and the English writing of this paper.

CONFLICT OF INTEREST

The authors declare that they have no conflicts of interest.

REFERENCES

1. X. Carton, *Surveys in Geophysics* **22**, 179 (2001).
2. X. Carton, *Lect. Notes in Phys.* **805**, 61 (2010).
3. D. B. Chelton, M. G. Schlax, R. M. Samelson, and R. A. de Szoeke, *Geophysical Research Letters* **34** (2007).
4. D. G. Dritschel, *Journal of Fluid Mechanics* **293**, 269 (1995).
5. M. A. Sokolovskiy and J. Verron, *Journal of Fluid Mechanics* **423**, 127 (2000).
6. J. N. Reinaud and D. G. Dritschel, *Journal of Fluid Mechanics* **469**, 287 (2002).
7. J. N. Reinaud and D. G. Dritschel, *Journal of Fluid Mechanics* **522**, 357 (2005).
8. J. N. Reinaud and X. Carton, *Journal of Fluid Mechanics* **636**, 109 (2009).
9. M. A. Sokolovskiy, K. V. Koshel, and X. Carton, *Geophysical & Astrophysical Fluid Dynamics* **105**, 506 (2011).
10. X. Carton, M. Morvan, J. N. Reinaud, M. A. Sokolovskiy, P. L'Hegaret, and C. Vic, *Regular and Chaotic Dynamics* **22**, 455 (2017).
11. D. G. Dritschel, *Journal of Fluid Mechanics* **455**, 83 (2002).
12. H. Plotka and D. G. Dritschel, *J. Fluid Mech.* **723**, 40 (2012).
13. H. Aref and N. Pomphrey, *Phys. Lett. A* **78**, 297 (1980).
14. X. Perrot and X. Carton, *Discr. Cont. Dyn. Syst. B* **11**, 971 (2009).
15. K. V. Koshel and E. A. Ryzhov, *Phys.Lett.A* **376** (2012).
16. P. Newton, *Fluid Dyn. Res.* **46**, 031401 (2014).
17. K. V. Koshel, J. N. Reinaud, G. Riccardi, and E. A. Ryzhov, *Physics of Fluids* **30**, 096603 (2018).
18. K. V. Koshel, E. A. Ryzhov, and X. J. Carton, *Fluids* **4**, 1 (2019).
19. M. A. Sokolovskiy, X. J. Carton, and B. N. Filyushkin, *Mathematics* **8**, 1228 (2020).
20. L. Renault, J. C. McWilliams, and J. Gula, *Sci. Rep.* **8**, 13388 (2018).
21. L. Renault, P. Marchesiello, S. Masson, and J. C. McWilliams, *Geophysical Research Letters* **46**, 2743 (2019).
22. A. V. Borisov and I. S. Mamaev, *Regular and Chaotic Dynamics* **11**, 455 (2006).
23. I. A. Bizyaev, A. V. Borisov, and I. S. Mamaev, *Regular and Chaotic Dynamics* **21**, 367 (2016).
24. X. Perrot and X. Carton, *Theoret. Comput. Fluid Dyn.* **24**, 95 (2010).